CLNS 07/2014
CLEO 07-18

# Determination of the $D^0 \to K^+\pi^-$ Relative Strong Phase Using Quantum-Correlated Measurements in $e^+e^- \to D^0\bar{D}^0$ at CLEO

D. M. Asner,[1] K. W. Edwards,[1] P. Naik,[1] R. A. Briere,[2] T. Ferguson,[2] G. Tatishvili,[2] H. Vogel,[2] M. E. Watkins,[2] J. L. Rosner,[3] J. P. Alexander,[4] D. G. Cassel,[4] J. E. Duboscq,[4] R. Ehrlich,[4] L. Fields,[4] L. Gibbons,[4] R. Gray,[4] S. W. Gray,[4] D. L. Hartill,[4] B. K. Heltsley,[4] D. Hertz,[4] C. D. Jones,[4] J. Kandaswamy,[4] D. L. Kreinick,[4] V. E. Kuznetsov,[4] H. Mahlke-Krüger,[4] D. Mohapatra,[4] P. U. E. Onyisi,[4] J. R. Patterson,[4] D. Peterson,[4] D. Riley,[4] A. Ryd,[4] A. J. Sadoff,[4] X. Shi,[4] S. Stroiney,[4] W. M. Sun,[4] T. Wilksen,[4] S. B. Athar,[5] R. Patel,[5] J. Yelton,[5] P. Rubin,[6] B. I. Eisenstein,[7] I. Karliner,[7] S. Mehrabyan,[7] N. Lowrey,[7] M. Selen,[7] E. J. White,[7] J. Wiss,[7] R. E. Mitchell,[8] M. R. Shepherd,[8] D. Besson,[9] T. K. Pedlar,[10] D. Cronin-Hennessy,[11] K. Y. Gao,[11] J. Hietala,[11] Y. Kubota,[11] T. Klein,[11] B. W. Lang,[11] R. Poling,[11] A. W. Scott,[11] P. Zweber,[11] S. Dobbs,[12] Z. Metreveli,[12] K. K. Seth,[12] A. Tomaradze,[12] J. Libby,[13] A. Powell,[13] G. Wilkinson,[13] K. M. Ecklund,[14] W. Love,[15] V. Savinov,[15] A. Lopez,[16] H. Mendez,[16] J. Ramirez,[16] J. Y. Ge,[17] D. H. Miller,[17] B. Sanghi,[17] I. P. J. Shipsey,[17] B. Xin,[17] G. S. Adams,[18] M. Anderson,[18] J. P. Cummings,[18] I. Danko,[18] D. Hu,[18] B. Moziak,[18] J. Napolitano,[18] Q. He,[19] J. Insler,[19] H. Muramatsu,[19] C. S. Park,[19] E. H. Thorndike,[19] F. Yang,[19] M. Artuso,[20] S. Blusk,[20] S. Khalil,[20] J. Li,[20] R. Mountain,[20] S. Nisar,[20] K. Randrianarivony,[20] N. Sultana,[20] T. Skwarnicki,[20] S. Stone,[20] J. C. Wang,[20] L. M. Zhang,[20] G. Bonvicini,[21] D. Cinabro,[21] M. Dubrovin,[21] A. Lincoln,[21] and J. Rademacker[22]

(CLEO Collaboration)

[1]*Carleton University, Ottawa, Ontario, Canada K1S 5B6*
[2]*Carnegie Mellon University, Pittsburgh, Pennsylvania 15213, USA*
[3]*Enrico Fermi Institute, University of Chicago, Chicago, Illinois 60637, USA*
[4]*Cornell University, Ithaca, New York 14853, USA*
[5]*University of Florida, Gainesville, Florida 32611, USA*
[6]*George Mason University, Fairfax, Virginia 22030, USA*
[7]*University of Illinois, Urbana-Champaign, Illinois 61801, USA*
[8]*Indiana University, Bloomington, Indiana 47405, USA*
[9]*University of Kansas, Lawrence, Kansas 66045, USA*
[10]*Luther College, Decorah, Iowa 52101, USA*
[11]*University of Minnesota, Minneapolis, Minnesota 55455, USA*
[12]*Northwestern University, Evanston, Illinois 60208, USA*
[13]*University of Oxford, Oxford OX1 3RH, UK*
[14]*State University of New York at Buffalo, Buffalo, New York 14260, U SA*
[15]*University of Pittsburgh, Pittsburgh, Pennsylvania 15260, USA*
[16]*University of Puerto Rico, Mayaguez, Puerto Rico 00681*
[17]*Purdue University, West Lafayette, Indiana 47907, USA*
[18]*Rensselaer Polytechnic Institute, Troy, New York 12180, USA*
[19]*University of Rochester, Rochester, New York 14627, USA*
[20]*Syracuse University, Syracuse, New York 13244, USA*
[21]*Wayne State University, Detroit, Michigan 48202, USA*
[22]*University of Bristol, Bristol BS8 1TL, UK*

(Dated: February 14, 2008)


## Abstract

We exploit the quantum coherence between pair-produced $D^0$ and $\bar{D}^0$ in $\psi(3770)$ decays to study charm mixing, which is characterized by the parameters $x$ and $y$, and to make a first determination of the relative strong phase $\delta$ between $D^0 \to K^+\pi^-$ and $\bar{D}^0 \to K^+\pi^-$. Using 281 pb$^{-1}$ of $e^+e^-$ collision data collected with the CLEO-c detector at $E_{\rm cm} = 3.77$ GeV, as well as branching fraction input from other experiments, we find $\cos\delta = 1.03^{+0.31}_{-0.17} \pm 0.06$, where the uncertainties are statistical and systematic, respectively. In addition, by further including external measurements of charm mixing parameters, we obtain an alternate measurement of $\cos\delta = 1.10 \pm 0.35 \pm 0.07$, as well as $x \sin\delta = (4.4^{+2.7}_{-1.8} \pm 2.9) \times 10^{-3}$ and $\delta = (22^{+11+9}_{-12-11})^\circ$.

## I. INTRODUCTION

Recent measurements of $D^0$-$\bar{D}^0$ mixing parameters [1–4] highlight the need for information on the relative phase between the Cabibbo-favored decay $D^0 \to K^-\pi^+$ and the doubly Cabibbo-suppressed (DCS) decay $\bar{D}^0 \to K^-\pi^+$. Here, we present a measurement that takes advantage of the correlated production of $D^0$ and $\bar{D}^0$ mesons in $e^+e^-$ collisions. If there are no accompanying particles, the $D^0\bar{D}^0$ pair is in a quantum-coherent $C = -1$ state. Because the initial state (the virtual photon) has $J^{PC} = 1^{--}$, there follows a set of selection rules for the decays of the $D^0$ and $\bar{D}^0$ [5–15]. For example, both $D^0$ and $\bar{D}^0$ cannot decay to $CP$ eigenstates with the same eigenvalue. On the other hand, decays to $CP$ eigenstates of opposite eigenvalue are enhanced by a factor of two. More generally, final states that can be reached by both $D^0$ and $\bar{D}^0$ (such as $K^-\pi^+$) are subject to similar interference effects. As a result, the effective $D^0$ branching fractions in this $D^0\bar{D}^0$ system differ from those measured in isolated $D^0$ mesons. Moreover, using time-independent rate measurements, it becomes possible to probe $D^0$-$\bar{D}^0$ mixing as well as the relative strong phases between $D^0$ and $\bar{D}^0$ decay amplitudes to any given final state.

In the Standard Model, $D^0$-$\bar{D}^0$ mixing is suppressed both by the GIM mechanism and by CKM matrix elements, although sizeable mixing could arise from new physics [14]. Charm mixing is conventionally described by two small dimensionless parameters:

$$x = 2\frac{M_2 - M_1}{\Gamma_2 + \Gamma_1} \tag{1}$$

$$y = \frac{\Gamma_2 - \Gamma_1}{\Gamma_2 + \Gamma_1}, \tag{2}$$

where $M_{1,2}$ and $\Gamma_{1,2}$ are the masses and widths, respectively, of the neutral $D$ meson $CP$ eigenstates, $D_1$ ($CP$-odd) and $D_2$ ($CP$-even), which are defined as follows:

$$|D_1\rangle \equiv \frac{|D^0\rangle + |\bar{D}^0\rangle}{\sqrt{2}} \tag{3}$$

$$|D_2\rangle \equiv \frac{|D^0\rangle - |\bar{D}^0\rangle}{\sqrt{2}}, \tag{4}$$

assuming $CP$ conservation. The mixing probability is then denoted by $R_{\rm M} \equiv (x^2 + y^2)/2$, and the width of the $D^0$ and $\bar{D}^0$ flavor eigenstates is $\Gamma \equiv (\Gamma_1 + \Gamma_2)/2$.

Many previous searches for charm mixing have focused on $D^0$ decay times. Direct measurements of $y$ come from comparing lifetimes in $D^0 \to K^+K^-$ and $\pi^+\pi^-$ decay to that in $D^0 \to K^-\pi^+$. An indirect measure of $y$ is provided by the "wrong-sign" process $D^0 \to K^+\pi^-$, where interference between the DCS amplitude and the mixing amplitude manifests itself in the apparent $D^0$ lifetime. These analyses are sensitive to $y' \equiv y\cos\delta - x\sin\delta$, where $-\delta$ is the phase of the amplitude ratio $\langle K^+\pi^-|D^0\rangle/\langle K^+\pi^-|\bar{D}^0\rangle \equiv re^{-i\delta}$. We adopt a convention in which $\delta$ corresponds to a strong phase, which vanishes in the SU(3) limit [13]. Because $\delta$ has not previously been measured, the separate determinations of $y$ and $y'$ above have not been directly comparable. The magnitude $r$ of the amplitude ratio is approximately 0.06.

In this article, we present an implementation of the method described in Ref. [16] for measuring $y$ and $\delta$ using quantum correlations at the $\psi(3770)$ resonance. Our experimental technique is an extension of the double tagging method previously used to determine

absolute hadronic $D$-meson branching fractions at CLEO-c [17]. This method combines yields of fully reconstructed single tags (ST), which are individually reconstructed $D^0$ or $\bar{D}^0$ candidates, with yields of double tags (DT), which are events where both $D^0$ and $\bar{D}^0$ are reconstructed, to give absolute branching fractions without needing to know the luminosity or $D^0\bar{D}^0$ production cross section. Given a set of input yields, efficiencies, and background estimates, a least-squares fitter [18] extracts the number of $D^0\bar{D}^0$ pairs produced ($\mathcal{N}$) and the branching fractions ($\mathcal{B}$) of the reconstructed $D^0$ final states, while accounting for all statistical and systematic uncertainties and their correlations. We employ a modified version of this fitter that also determines $y$, $x^2$, $r^2$, $r\cos\delta$, and $rx\sin\delta$ using the following categories of reconstructed final states: $K^-\pi^+$ ($f$), $K^+\pi^+$ ($\bar{f}$), $CP$-even ($S_+$) and $CP$-odd ($S_-$) eigenstates, and semileptonic decays ($e^\pm$). For optimal precision on $\delta$, we also incorporate measurements of branching fractions and mixing parameters from other CLEO-c analyses or from external sources. We neglect $CP$ violation in $D$ decays, which would entail a slight correction to the mixing signal.

The paper is organized as follows. In Section II, we review the formalism of quantum-correlated $D^0\bar{D}^0$ decay. Section III describes the event selection criteria and $D$ reconstruction procedures. The external measurements used in the fit are summarized in Section IV. Systematic uncertainties, which are also input to the fit, are discussed in Section V. Finally, we present and discuss our fit results in Section VI.

## II. FORMALISM

To first order in $x$ and $y$, the $C$-odd rate $\Gamma_{D^0\bar{D}^0}(i,j)$ for $D^0\bar{D}^0$ decay to final state $\{i,j\}$ follows from the anti-symmetric amplitude $\mathcal{M}_{ij}$:

$$\begin{aligned}\Gamma_{D^0\bar{D}^0}(i,j) \propto \mathcal{M}_{ij}^2 &= \left|A_i\bar{A}_j - \bar{A}_i A_j\right|^2 \\ &= \left|\langle i|D_2\rangle\langle j|D_1\rangle - \langle i|D_1\rangle\langle j|D_2\rangle\right|^2, \end{aligned} \tag{5}$$

where $A_i \equiv \langle i|D^0\rangle$ and $\bar{A}_i \equiv \langle i|\bar{D}^0\rangle$. These amplitudes are normalized such that $\mathcal{B}_{K^-\pi^+} \approx A^2_{K^-\pi^+}(1 + ry\cos\delta + rx\sin\delta)$, $\mathcal{B}_{S_\pm} \approx A^2_{S_\pm}(1 \mp y)$, and $\mathcal{B}_e \approx A_e^2$. The total rate, $\Gamma_{D^0\bar{D}^0}$, is the same as for uncorrelated decay, as are ST rates. However, unlike the case of uncorrelated $D^0\bar{D}^0$, we can consider the $C$-odd $D^0\bar{D}^0$ system as a $D_1D_2$ pair. If only flavored final states are considered, as in Ref. [17], then the effects of quantum correlations are negligible. In this analysis, we also include $CP$ eigenstates, which brings additional sensitivity to $y$ and $\delta$, as demonstrated below.

Quantum-correlated semileptonic rates probe $y$ because the decay width does not depend on the $CP$ eigenvalue of the parent $D$ meson, as this weak decay is only sensitive to flavor content. However, the total width of the parent meson does depend on its $CP$ eigenvalue: $\Gamma_1 = \Gamma(1 \mp y)$, so the semileptonic branching fraction for $D_1$ or $D_2$ is modified by $1 \pm y$. If we reconstruct a semileptonic decay in the same event as a $D_2 \to S_+$ decay, then the semileptonic $D$ must be a $D_1$. Therefore, the effective quantum-correlated $D^0\bar{D}^0$ branching fractions ($\mathcal{F}^{\rm cor}$) for $\{S_\pm, e\}$ final states depend on $y$:

$$\mathcal{F}^{\rm cor}_{S_\pm,e} \approx 2\mathcal{B}_{S_\pm}\mathcal{B}_e(1 \pm y), \tag{6}$$

where the factor of 2 arises from the sum of $e^+$ and $e^-$ rates. Combined with estimates of $\mathcal{B}_e$ and $\mathcal{B}_{S_\pm}$ from ST yields, external sources, and flavor-tagged semileptonic yields, this equation allows $y$ to be determined.

Similarly, if we reconstruct a $D \to K^-\pi^+$ decay in the same event as a $D_2 \to S_+$, then the $K^-\pi^+$ was produced from a $D_1$. The effective branching fraction for this DT process is therefore

$$\begin{aligned}
\mathcal{F}^{\rm cor}_{S_+,K^-\pi^+} &= |\langle S_+|D_2\rangle\langle K^-\pi^+|D_1\rangle|^2 \\
&\approx \mathcal{B}_{S_+}(1+y)|A_{K^-\pi^+} + \bar{A}_{K^-\pi^+}|^2 \\
&\approx \mathcal{B}_{S_+}\mathcal{B}_{K^-\pi^+}(1+y)(1-ry\cos\delta - rx\sin\delta)|1+re^{-i\delta}|^2 \\
&= \mathcal{B}_{S_+}\mathcal{B}_{K^-\pi^+}(1+y)(1-ry\cos\delta - rx\sin\delta)(1+2r\cos\delta + r^2) \\
&\approx \mathcal{B}_{S_+}\mathcal{B}_{K^-\pi^+}(1+2r\cos\delta + R_{\rm WS} + y), \qquad (7)
\end{aligned}$$

where $R_{\rm WS}$ is the wrong-sign rate ratio, which depends on $x$ and $y$ because of the interference between DCS and mixing transitions: $R_{\rm WS} \equiv \Gamma(\bar{D}^0 \to K^-\pi^+)/\Gamma(D^0 \to K^-\pi^+) = r^2 + ry' + R_{\rm M}$. In an analogous fashion, we find $\mathcal{F}^{\rm cor}_{S_-,K^-\pi^+} \approx \mathcal{B}_{S_-}\mathcal{B}_{K^-\pi^+}(1+R_{\rm WS}-2r\cos\delta - y)$. When combined with knowledge of $\mathcal{B}_{S_+}$, $y$, and $r$, the asymmetry between these two DT yields gives $\cos\delta$. In the absence of quantum correlations, the effective branching fractions above would be $\mathcal{B}_{S_\pm}\mathcal{B}_{K^-\pi^+}(1+R_{\rm WS})$.

More concretely, we evaluate Eq. (5) with the above definitions of $r$ and $\delta$ to produce the expressions in Table I. In doing so, we use the fact that inclusive ST rates are given by the incoherent branching fractions since each event contains one $D^0$ and one $\bar{D}^0$. Comparison of $\mathcal{F}^{\rm cor}$ with the uncorrelated effective branching fractions, $\mathcal{F}^{\rm unc}$, also given in Table I, allows us to extract $r^2$, $r\cos\delta$, $y$, $x^2$, and $rx\sin\delta$. Information on $\mathcal{B}_i$ is obtained from ST yields at the $\psi(3770)$ and from external measurements using incoherently produced $D^0$ mesons. These two estimates of $\mathcal{B}_i$ are averaged by the fitter to obtain $\mathcal{F}^{\rm unc}$.

TABLE I: Correlated ($C$-odd) and uncorrelated effective $D^0\bar{D}^0$ branching fractions, $\mathcal{F}^{\rm cor}$ and $\mathcal{F}^{\rm unc}$, to leading order in $x$, $y$ and $R_{\rm WS}$, divided by $\mathcal{B}_i$ for ST modes $i$ (first section) and $\mathcal{B}_i\mathcal{B}_j$ for DT modes $\{i,j\}$ (second section). Charge conjugate modes are implied.

| Mode | Correlated | Uncorrelated |
|---|---|---|
| $K^-\pi^+$ | $1+R_{\rm WS}$ | $1+R_{\rm WS}$ |
| $S_+$ | 2 | 2 |
| $S_-$ | 2 | 2 |
| $K^-\pi^+, K^-\pi^+$ | $R_{\rm M}$ | $R_{\rm WS}$ |
| $K^-\pi^+, K^+\pi^-$ | $(1+R_{\rm WS})^2 - 4r\cos\delta(r\cos\delta + y)$ | $1+R^2_{\rm WS}$ |
| $K^-\pi^+, S_+$ | $1+R_{\rm WS}+2r\cos\delta+y$ | $1+R_{\rm WS}$ |
| $K^-\pi^+, S_-$ | $1+R_{\rm WS}-2r\cos\delta-y$ | $1+R_{\rm WS}$ |
| $K^-\pi^+, e^-$ | $1-ry\cos\delta - rx\sin\delta$ | 1 |
| $S_+, S_+$ | 0 | 1 |
| $S_-, S_-$ | 0 | 1 |
| $S_+, S_-$ | 4 | 2 |
| $S_+, e^-$ | $1+y$ | 1 |
| $S_-, e^-$ | $1-y$ | 1 |

Using only ST and DT yields at the $\psi(3770)$, we can determine $y$ and $\cos\delta$ from the

following double ratios, obtained by manipulating the expressions in Table I:

$$y \approx \frac{N_{fe}}{4N_f}\left[\frac{N_{S_-}}{N_{S_-e}} - \frac{N_{S_+}}{N_{S_+e}}\right] \quad (8)$$

$$\approx \frac{1}{4}\left[\frac{N_{S_+e}N_{S_-}}{N_{S_-e}N_{S_+}} - \frac{N_{S_-e}N_{S_+}}{N_{S_+e}N_{S_-}}\right] \quad (9)$$

$$2r\cos\delta + y \approx \frac{N_{f\bar{f}}}{4N_{\bar{f}}}\left[\frac{N_{S_-}}{N_{S_-f}} - \frac{N_{S_+}}{N_{S_+f}}\right] \quad (10)$$

$$\approx \frac{1}{4}N_f N_{S_+S_-}\left[\frac{1}{N_{fS_-}N_{S_+}} - \frac{1}{N_{fS_+}N_{S_-}}\right], \quad (11)$$

where $N$ denotes an efficiency-corrected background-subtracted ST or DT yield. Note that semileptonic yields are essential for separating $y$ and $\cos\delta$. Including external branching fractions provides additional ways to determine $y$ and $\cos\delta$:

$$y = \pm\left[1 - \frac{2\mathcal{N}\mathcal{B}_{S_\pm}\mathcal{B}_e}{N_{S_\pm e}}\right] \quad (12)$$

$$2r\cos\delta + y = (1 + R_{\rm WS})\left[\frac{N_{S_+f}/\mathcal{B}_{S_+} - N_{S_-f}/\mathcal{B}_{S_-}}{N_{S_+f}/\mathcal{B}_{S_+} + N_{S_-f}/\mathcal{B}_{S_-}}\right]. \quad (13)$$

Although we neglect $x^2$ and $y^2$ terms in general, we report a result for $x^2$ as determined solely from $N_{ff}/N_{f\bar{f}}$.

## III. EVENT SELECTION AND RECONSTRUCTION

Our current analysis uses 281 pb$^{-1}$ of $e^+e^- \to \psi(3770)$ data collected with the CLEO-c [19–23] detector. We also make use of a large Monte Carlo simulated sample of uncorrelated $D^0\bar{D}^0$ decays with an effective luminosity 40 times that of our data sample, from which we estimate signal efficiencies, crossfeed probabilities among signal modes, and background contributions. In these samples, we reconstruct the final states shown in Table II, with $\pi^0 \to \gamma\gamma$, $\eta \to \gamma\gamma$, $K^0_S \to \pi^+\pi^-$, and $\omega \to \pi^+\pi^-\pi^0$. Because most $K^0_L$ mesons and neutrinos are not detected, we do not reconstruct $K^0_L\pi^0$ and semileptonic ST modes; they are only included in DT modes, paired with a fully reconstructed $D$ candidate. Below, we denote by $S'_+$ the subset of $S_+$ modes that are fully reconstructed: $K^+K^-$, $\pi^+\pi^-$, and $K^0_S\pi^0\pi^0$. For $CP$ eigenstates, we choose modes with unambiguous $CP$ content. In addition to two-body decays, we also include $K^0_S\pi^0\pi^0$, which is a pure $CP$-even eigenstate because the two identical $\pi^0$'s must have even angular momentum in order to satisfy Bose symmetry. We neglect $CP$ violation in $K^0$ decays.

Standard CLEO-c selection critera for $\pi^\pm$, $K^\pm$, $\pi^0$, and $K^0_S$ candidates are described in Ref. [24]. In addition, for $K^0_S$ candidates, we impose $|M(\pi^+\pi^-) - M_{K^0_S}| < 7.5$ MeV/$c^2$, and we require the decay vertex to be separated from the interaction region with a significance greater than two standard deviations ($\sigma$). For the $K^0_S\pi^0\pi^0$ mode, we reject $K^0_S$ daughter tracks with ionization energy loss consistent with being kaons at the level of $2\sigma$ in order to suppress misreconstructed $D \to K^-\pi^+\pi^0$ decays, where the kaon is taken to be a charged pion, and an extra soft combinatoric $\pi^0$ candidate is incorporated into the $D$ candidate. We

TABLE II: $D$ final states reconstructed in this analysis.

| Type | Final States |
|---|---|
| Flavored | $K^-\pi^+$, $K^+\pi^-$ |
| $S_+$ | $K^+K^-$, $\pi^+\pi^-$, $K^0_S\pi^0\pi^0$, $K^0_L\pi^0$ |
| $S_-$ | $K^0_S\pi^0$, $K^0_S\eta$, $K^0_S\omega$ |
| $e^\pm$ | Inclusive $Xe^+\nu_e$, $Xe^-\bar{\nu}_e$ |

accept $\omega$ candidates with $|M(\pi^+\pi^-\pi^0) - M_\omega| < 20$ MeV/$c^2$. Reconstruction of $\eta \to \gamma\gamma$ proceeds analogously to $\pi^0 \to \gamma\gamma$. In addition, we require $|M(\gamma\gamma) - M_\eta| < 42$ MeV/$c^2$. All invariant mass requirements correspond to approximately $3\sigma$ consistency with the nominal masses from Ref. [25].

### 1. *Single Tags*

Reconstruction of all modes in this analysis, including DT modes, begins with fully reconstructed ST $D$ candidates, which are identified using two kinematic variables that express momentum and energy conservation: the beam-constrained candidate mass $M$ and the energy difference $\Delta E$. These variables are defined to be

$$M \equiv \sqrt{E_0^2/c^4 - \mathbf{p}_D^2/c^2} \tag{14}$$

$$\Delta E \equiv E_D - E_0, \tag{15}$$

where $\mathbf{p}_D$ and $E_D$ are the total momentum and energy of the $D$ candidate, and $E_0$ is the beam energy. Correctly reconstructed $D$ candidates produce a peak in $M$ at the $D$ mass and in $\Delta E$ at zero. We determine ST yields by fitting the $M$ distribution with the mode-dependent requirements on $\Delta E$ listed in Table III, which are applied to both ST and DT $D$ candidates. The limits are set at approximately three standard deviations. Modes with $\pi^0$ or $\eta$, which decay to two photons, have asymmetric limits to allow for partially contained showers in the electromagnetic calorimeter.

TABLE III: Requirements on $\Delta E$ for $D$ candidates.

| Mode | Requirement (GeV) |
|---|---|
| $K^-\pi^+$ | $\lvert\Delta E\rvert < 0.0294$ |
| $K^+\pi^-$ | $\lvert\Delta E\rvert < 0.0294$ |
| $K^+K^-$ | $\lvert\Delta E\rvert < 0.0200$ |
| $\pi^+\pi^-$ | $\lvert\Delta E\rvert < 0.0300$ |
| $K^0_S\pi^0\pi^0$ | $-0.0550 < \Delta E < 0.0450$ |
| $K^0_S\pi^0$ | $-0.0710 < \Delta E < 0.0450$ |
| $K^0_S\eta$ | $-0.0550 < \Delta E < 0.0350$ |
| $K^0_S\omega$ | $\lvert\Delta E\rvert < 0.0250$ |

For $K^\pm\pi^\mp$, $K^+K^-$, and $\pi^+\pi^-$ ST modes, in events containing only two tracks, we suppress cosmic muons and beam-energy Bhabhas by vetoing tracks that are identified as muons or electrons and by requiring at least one electromagnetic shower in the calorimeter above 50

MeV not associated with the signal tracks. For $K^+K^-$ ST candidates, additional geometric requirements are needed to remove doubly radiative Bhabhas followed by pair conversion of a radiated photon. Also, we accept only one candidate per mode per event; when multiple candidates are present, we choose the one with smallest $|\Delta E|$.

The resultant $M$ distributions, shown in Fig. 1, are fitted to a signal shape derived from simulated signal events and to a background ARGUS function [26]. The simulated signal shape is both shifted and convoluted with a Gaussian smearing function to account for imperfect modeling of the detector resolution and beam energy calibration. The width of the smearing function is allowed to float in the fit. The measured ST yields and efficiencies are given in Table IV. The yield uncertainties are statistical and uncorrelated systematic, respectively. The latter arise from modeling of multiple candidates in simulation and variations in the signal lineshape. Correlated systematic uncertainties are discussed separately in Section V.

TABLE IV: ST yields and efficiencies input to the data fit. Yield uncertainties are statistical and uncorrelated systematic, respectively, and efficiency uncertainties are statistical only.

| Mode | Yield | Efficiency (%) |
|---|---|---|
| $K^-\pi^+$ | $25374 \pm 166 \pm 26$ | $64.70 \pm 0.04$ |
| $K^+\pi^-$ | $25842 \pm 167 \pm 26$ | $65.62 \pm 0.04$ |
| $K^+K^-$ | $4740 \pm 71 \pm 5$ | $57.25 \pm 0.09$ |
| $\pi^+\pi^-$ | $2098 \pm 59 \pm 9$ | $72.92 \pm 0.13$ |
| $K^0_S\pi^0\pi^0$ | $2435 \pm 72 \pm 16$ | $12.50 \pm 0.06$ |
| $K^0_S\pi^0$ | $7523 \pm 91 \pm 17$ | $29.73 \pm 0.05$ |
| $K^0_S\eta$ | $1051 \pm 39 \pm 17$ | $10.34 \pm 0.06$ |
| $K^0_S\omega$ | $3239 \pm 63 \pm 7$ | $12.48 \pm 0.04$ |

*2. Fully Reconstructed Hadronic Double Tags*

Except for modes with $K^0_L\pi^0$, we form hadronic DTs by combining two ST candidates passing the above selection criteria. Multiple candidates are resolved after forming the DT candidates, not at the ST level. We choose one candidate per mode per event with $\bar{M}$ closest to the measured $D^0$ mass, where $\bar{M} \equiv [M(D^0) + M(\bar{D}^0)]/2$. We extract signal yields by counting events in the two-dimensional $M(D^0)$ vs. $M(\bar{D}^0)$ plane, as illustrated in Fig. 2. The signal region S is defined to be approximately three standard deviations in each dimension: $1.86 < M(D^0) < 1.87$ GeV/$c^2$ and $1.86 < M(\bar{D}^0) < 1.87$ GeV/$c^2$. Sidebands A and B contain candidates where either the $D^0$ or the $\bar{D}^0$ is misreconstructed. Sidebands C and D contain candidates where both $D^0$ and $\bar{D}^0$ are misreconstructed, either in a correlated way (C) by assigning daughter particles to the wrong parent or in an uncorrelated way (D). Event counts in sidebands A, B, and C are projected into the signal region S using scale factors determined from integrating the background shape in the ST $M$ fits. Contributions to sideband D are assumed to be uniformly distributed across the other regions. We assign a conservative systematic uncertainty of 100% on the size of the sideband subtractions.

Table V gives the fully reconstructed DT yields and efficiencies input to the fit, and Fig. 3 shows the corresponding $\bar{M}$ projections. Same-$CP$ $\{S_\pm, S_\pm\}$ modes are not included in the standard fit.

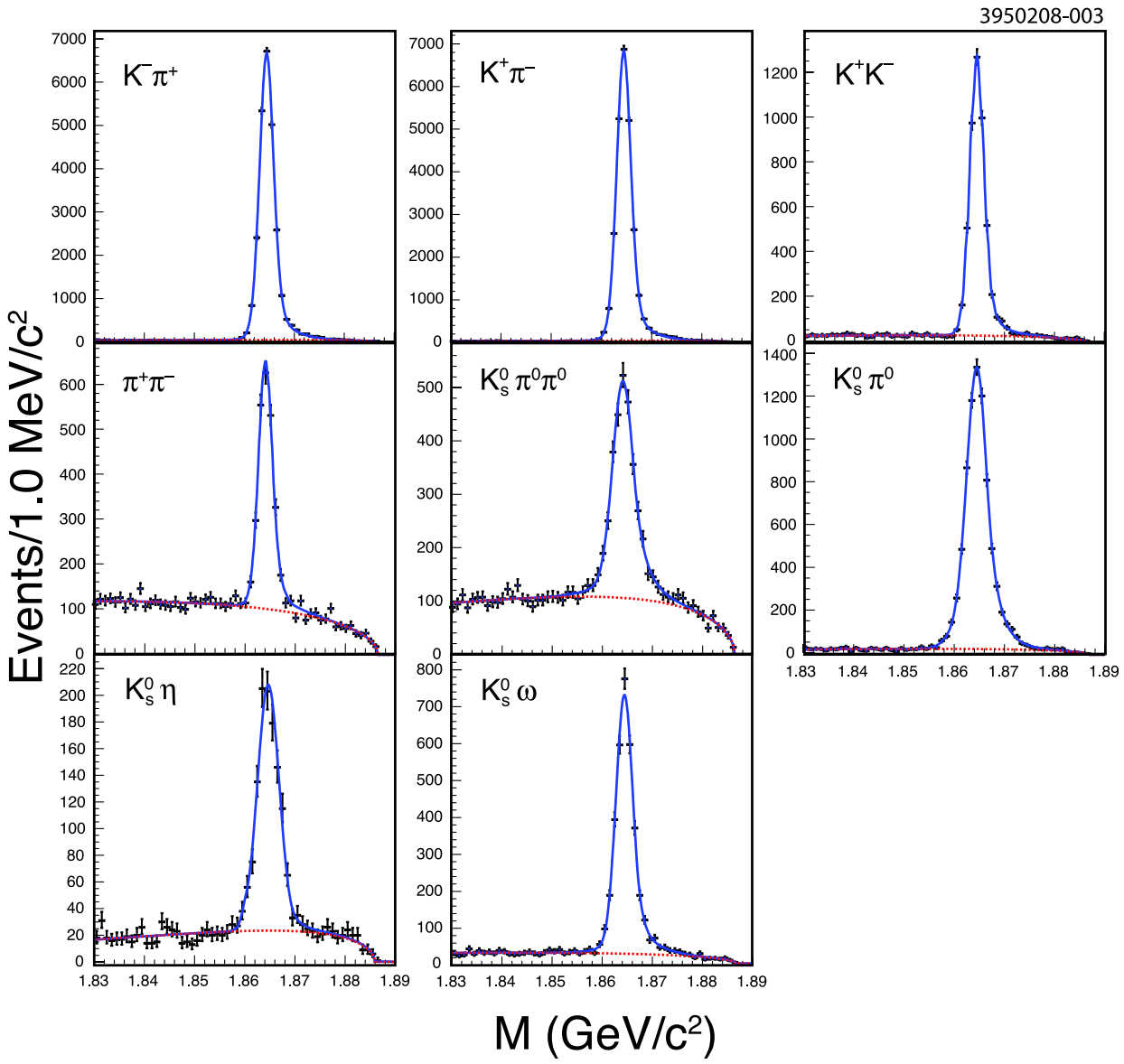


FIG. 1: ST $M$ distributions and fits. Data are shown as points with error bars. The solid lines show the total fits, and the dashed lines show the background shapes.

### *3. Semileptonic Double Tags*

Semileptonic DTs are partially reconstructed by combining a fully reconstructed hadronic ST with an electron candidate from the remainder of the event. The hadronic tags are selected using the same criteria as for STs, described in in Section III 1, with an additional mode-dependent $M$ requirement listed in Table VI. The limits are set at approximately three standard deviations. Multiple tag candidates are resolved with minimal $|\Delta E|$, as for STs. All electron candidates in a given event are accepted.

Electron candidate tracks must have momentum greater than 200 MeV/$c$ and impact parameters with respect to the event origin of less than 5 mm in the $r$-$\phi$ plane and less than 5 cm in the $z$ dimension. We also require the track to have more than half the hits expected for

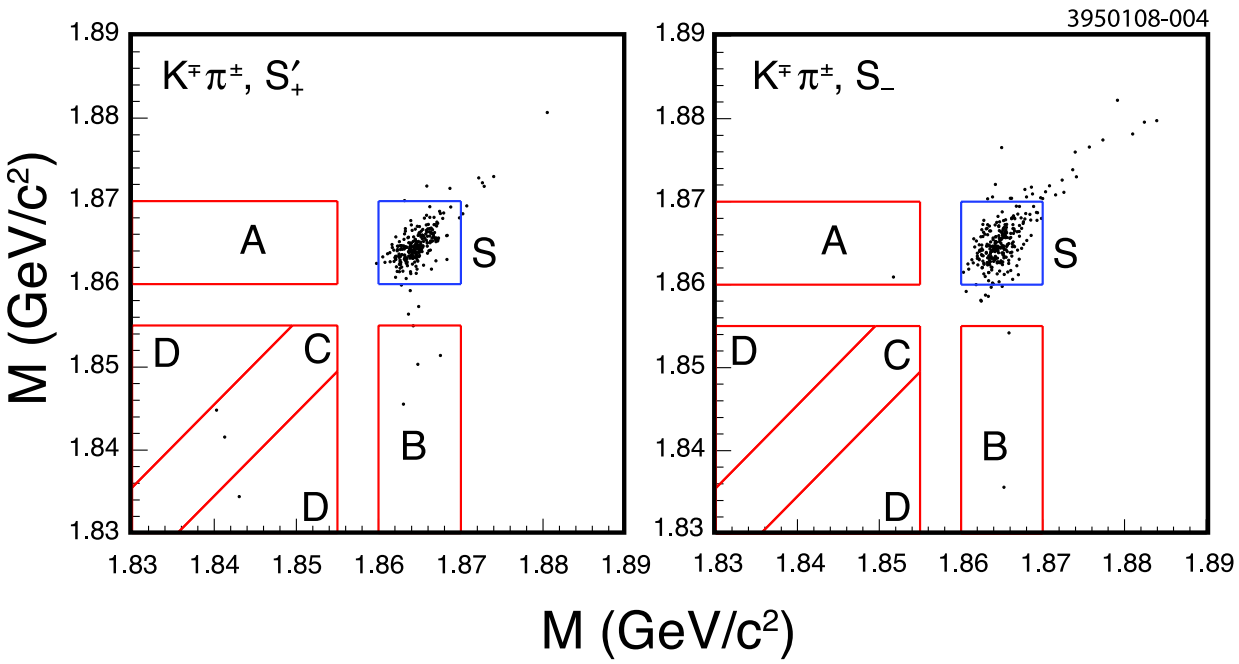


FIG. 2: Two-dimensional $M$ distributions with signal (S) and sideband (A, B, C, D) regions depicted, for the sum of all $\{K^{\mp}\pi^{\pm}, S'_{+}\}$ and $\{K^{\mp}\pi^{\pm}, S_{-}\}$ modes listed in Table V.

its momentum and to have $|\cos\theta| < 0.9$, where $\theta$ is the angle between the track momentum vector and the beam line at the interaction point. These criteria remove kinematic regions with high background. When paired with a $K^{\mp}\pi^{\pm}$ tag, the kaon and electron charges must be the same. This requirement removes charge-symmetric backgrounds and cannot be used with unflavored $S_{\pm}$ tag modes.

Electrons are distinguished from hadrons via a multivariate discriminant [27] that combines information from the ratio of the energy deposited in the calorimeter to the measured track momentum ($E/p$), ionization energy loss in the tracking chambers ($dE/dx$), and the ring-imaging Čerenkov counter (RICH). The ratio of electron likelihood to the sum of electron, pion, and kaon likelihoods is required to be greater than 0.8.

As illustrated in Fig. 4, the resulting electron momentum spectrum for each tag mode is fit to signal and background shapes determined from the simulation. We correct the simulated spectrum for relative bin-by-bin efficiency differences between data and simulation, which are measured with a high-statistics radiative Bhabha sample. The background components in the spectrum fit include misreconstructed tags, photon conversions and light hadron decays to electrons (mostly $\pi^0$ Dalitz decays), weak decays in flight, and hadron misidentification. The latter component peaks at 700 MeV/$c$ and mostly consists of $K^{\pm}$ that escape the acceptance of the RICH; $K^{\pm}$ are indistinguishable from $e^{\pm}$ using $dE/dx$ at this momentum. In the fit, the misreconstructed tag component is fixed from sidebands in $M$ and $\Delta E$. The other backgrounds contribute approximately 7% for $K^{\mp}\pi^{\pm}$ tags and 20–30% for $S_{\pm}$ tags.

Table VII gives the semileptonic DT yields and efficiencies input to the fit. The uncorrelated systematic uncertainties are determined from yield excursions under variation of the spectrum fit.

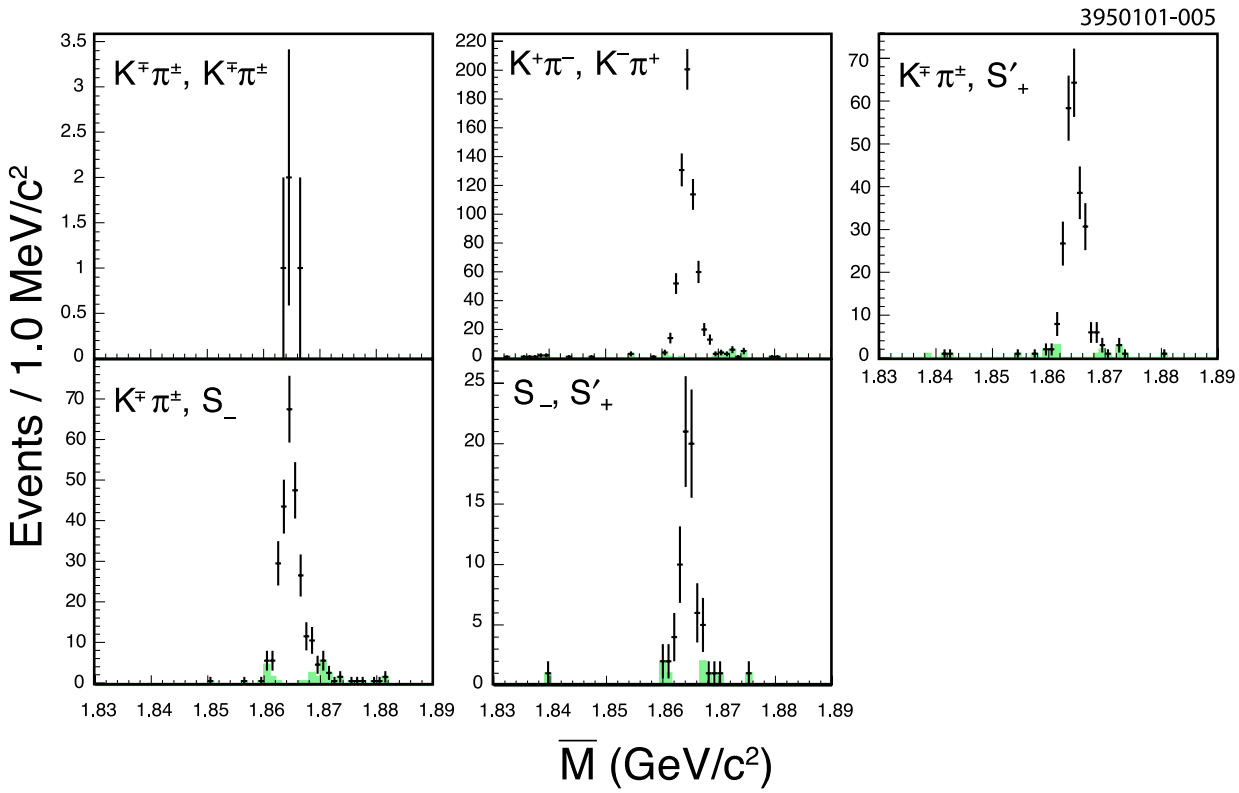


FIG. 3: Sums of fully reconstructed DT $\bar{M}$ distributions, with charge conjugate modes implied. Data are shown as points with error bars. The shaded histograms show events outside the signal region.

#### *4. Double Tags with $K^0_L\pi^0$*

DT modes with $K^0_L\pi^0$ are reconstructed with the missing mass technique also used in Ref. [28]. A fully reconstructed ST candidate, selected as described in Section III 1, is combined with a $\pi^0$ candidate, and we compute the squared recoil mass against the ST-$\pi^0$ system, $M^2_{\rm miss}$. Signal $K^0_L\pi^0$ decays produce a peak in $M^2_{\rm miss}$ at $M_{K^0_L}$. Backgrounds from $D \to K^0_S\pi^0$, $\pi^0\pi^0$, and $\eta\pi^0$ are suppressed by vetoing events with additional unassigned charged particles, $\eta$, or $\pi^0$ candidates.

Figure 5 shows the resultant $M^2_{\rm miss}$ in data. Signal yields are obtained from event counts in the signal region of $0.1 < M^2_{\rm miss} < 0.5$ GeV$^2/c^4$. The contribution from combinatoric background is estimated from the $0.8 < M^2_{\rm miss} < 1.2$ GeV$^2/c^4$ sideband to be $\mathcal{O}(10^{-3})$ and is subtracted. The residual background contributions from $K^0_S\pi^0$ and $\eta\pi^0$, which peak in the signal region, and from $\pi^0\pi^0$, which peaks below the signal region, are estimated from simulated data and are subtracted by the fitter, as described in Section III 5.

Table VIII lists the $K^0_L\pi^0$ DT yields and efficiencies input to the fit. There are no uncorrelated systematic uncertainties for these modes.

#### *5. Crossfeed and Peaking Backgrounds*

TABLE V: Fully reconstructed DT yields and efficiencies input to the data fit. Yield uncertainties are statistical and uncorrelated systematic (for sideband subtraction), respectively, and efficiency uncertainties are statistical only.

| Mode | Yield | Efficiency (%) |
|---|---|---|
| $K^-\pi^+, K^-\pi^+$ | $2.0 \pm 1.4 \pm 0$ | $36.1 \pm 3.4$ |
| $K^-\pi^+, K^+\pi^-$ | $600 \pm 25 \pm 5$ | $41.1 \pm 0.2$ |
| $K^-\pi^+, K^+K^-$ | $71 \pm 8 \pm 1$ | $35.5 \pm 0.6$ |
| $K^-\pi^+, \pi^+\pi^-$ | $24 \pm 5 \pm 1$ | $44.4 \pm 1.1$ |
| $K^-\pi^+, K^0_S\pi^0\pi^0$ | $32 \pm 6 \pm 1$ | $8.0 \pm 0.3$ |
| $K^-\pi^+, K^0_S\pi^0$ | $88 \pm 9 \pm 1$ | $18.4 \pm 0.3$ |
| $K^-\pi^+, K^0_S\eta$ | $8.0 \pm 2.8 \pm 0.0$ | $6.0 \pm 0.3$ |
| $K^-\pi^+, K^0_S\omega$ | $29 \pm 5 \pm 0$ | $8.7 \pm 0.2$ |
| $K^+\pi^-, K^+\pi^-$ | $2.0 \pm 1.4 \pm 0.0$ | $44.1 \pm 3.3$ |
| $K^+\pi^-, K^+K^-$ | $54 \pm 7 \pm 0$ | $36.1 \pm 0.6$ |
| $K^+\pi^-, \pi^+\pi^-$ | $25 \pm 5 \pm 1$ | $48.1 \pm 1.1$ |
| $K^+\pi^-, K^0_S\pi^0\pi^0$ | $33 \pm 6 \pm 0$ | $8.0 \pm 0.3$ |
| $K^+\pi^-, K^0_S\pi^0$ | $76 \pm 9 \pm 0$ | $18.6 \pm 0.3$ |
| $K^+\pi^-, K^0_S\eta$ | $9 \pm 3 \pm 0$ | $6.1 \pm 0.3$ |
| $K^+\pi^-, K^0_S\omega$ | $33 \pm 6 \pm 1$ | $8.0 \pm 0.2$ |
| $K^+K^-, K^0_S\pi^0$ | $39 \pm 6 \pm 1$ | $17.1 \pm 0.6$ |
| $K^+K^-, K^0_S\eta$ | $7.0 \pm 2.7 \pm 0.0$ | $7.1 \pm 0.8$ |
| $K^+K^-, K^0_S\omega$ | $20 \pm 4 \pm 0$ | $6.8 \pm 0.4$ |
| $\pi^+\pi^-, K^0_S\pi^0$ | $13 \pm 4 \pm 0$ | $19.2 \pm 1.2$ |
| $\pi^+\pi^-, K^0_S\eta$ | $2.0 \pm 1.4 \pm 0.0$ | $8.1 \pm 1.4$ |
| $\pi^+\pi^-, K^0_S\omega$ | $7.0 \pm 2.7 \pm 0.0$ | $9.9 \pm 0.9$ |
| $K^0_S\pi^0\pi^0, K^0_S\pi^0$ | $14 \pm 4 \pm 0$ | $3.5 \pm 0.2$ |
| $K^0_S\pi^0\pi^0, K^0_S\eta$ | $4.0 \pm 2.0 \pm 0.0$ | $1.2 \pm 0.2$ |
| $K^0_S\pi^0\pi^0, K^0_S\omega$ | $4.0 \pm 2.0 \pm 0.0$ | $1.4 \pm 0.2$ |

The yields in Tables IV, V, VII, and VIII include peaking backgrounds contributions and crossfeed among signal modes that are subtracted by the fitter. To do so, the fitter makes use of crossfeed probabilities and background efficiencies determined from simulated events, as well as branching fractions for peaking background processes [25]. These inputs are listed in Table IX. The correlated uncertainties among these contributions is also accounted for.

In most cases, the peaking background processes produce the same final state particles as the signal modes to which they contribute. For these backgrounds, the DT contribution is assumed to occur at the same rate as for STs. Other backgrounds, indicated by asterisks in Table IX, arise from misreconstructed $D$ decays. These backgrounds are present only in ST modes and do not contribute to DT modes because of the kinematic constraints of full event reconstruction. Background processes are identified using simulated $D^0\bar{D}^0$ events, where each $D$ is uncorrelated with the other and decays generically. Background efficiencies are determined by observing the change in signal yield as each background contribution is removed from the simulated sample.

We also adjust the peaking background estimates for quantum correlation effects. The

TABLE VI: Requirements on $M$ for hadronic tags in semileptonic DT candidates

| Mode | Requirement (GeV/$c^2$) |
|---|---|
| $K^-\pi^+$ | $1.8585 < M < 1.8775$ |
| $K^+\pi^-$ | $1.8585 < M < 1.8775$ |
| $K^+K^-$ | $1.8585 < M < 1.8775$ |
| $\pi^+\pi^-$ | $1.8585 < M < 1.8775$ |
| $K^0_S\pi^0\pi^0$ | $1.8530 < M < 1.8780$ |
| $K^0_S\pi^0$ | $1.8530 < M < 1.8780$ |
| $K^0_S\eta$ | $1.8585 < M < 1.8775$ |
| $K^0_S\omega$ | $1.8585 < M < 1.8775$ |

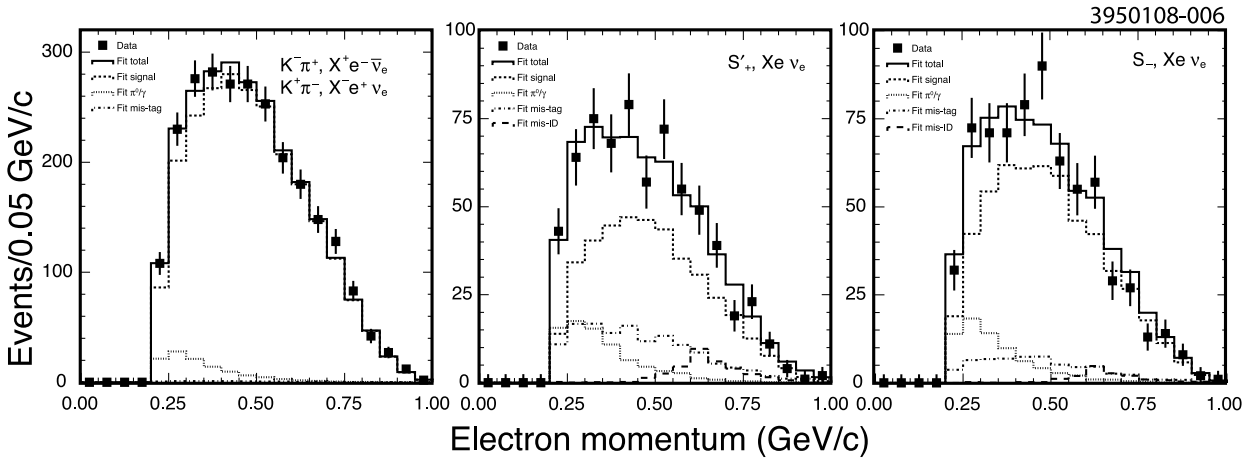


FIG. 4: Sums of electron momentum spectra for $X^-e^+\nu_e$ and $X^+e^-\bar{\nu}_e$. Data are shown as points with error bars, and the histograms show the signal and background components in the fits.

background branching fractions and efficiencies mentioned above assume uncorrelated $D$ decay, but the background estimate also depends on the type of decay of the other $D$. For instance, $K^0_L\pi^0$ signals have crossfeed background from $K^0_S\pi^0$ but only for $K\pi$ and $CP$-even tags. In $K^0_L\pi^0$ candidates opposite $CP$-odd tags, $K^0_S\pi^0$ cannot contribute because it is also $CP$-odd. For non-$CP$-eigenstate multi-body backgrounds, we assume equal $CP$-eigenstate and flavored content, with the $CP$-eigenstate content equally divided between $CP$-even and $CP$-odd. Variations in these assumptions give rise to systematic uncertainties, which are assessed in Section VI. In general, peaking backgrounds account for less than 1% of the measured yields, except in $K^0_S\omega$ modes (5–10%), $K^0_L\pi^0$ modes (1–2%), and ST $K^0_S\pi^0\pi^0$ (3%).

## IV. EXTERNAL MEASUREMENTS

As discussed in Section II, external estimates of uncorrelated branching fractions can help determine $y$ and $\delta$. We include measurements from Refs. [25, 29] and from other CLEO-c analyses along with their full error matrix in the fit. For the CLEO-c analyses, we account for statistical correlations with the yields measured in this analysis. Tables X, XI, and XII

TABLE VII: Semileptonic DT yields and efficiencies input to the data fit. Yield uncertainties are statistical and uncorrelated systematic, respectively, and efficiency uncertainties are statistical only.

| Mode | Yield | Efficiency (%) |
|---|---|---|
| $X^+e^-\bar{\nu}_e, K^-\pi^+$ | $1128 \pm 45 \pm 13$ | $45.3 \pm 0.2$ |
| $X^+e^-\bar{\nu}_e, K^-K^+$ | $128 \pm 24 \pm 5$ | $40.1 \pm 0.5$ |
| $X^+e^-\bar{\nu}_e, \pi^-\pi^+$ | $49 \pm 12 \pm 7$ | $50.3 \pm 0.9$ |
| $X^+e^-\bar{\nu}_e, K^0_S\pi^0\pi^0$ | $37 \pm 22 \pm 12$ | $8.9 \pm 0.2$ |
| $X^+e^-\bar{\nu}_e, K^0_S\pi^0$ | $195 \pm 24 \pm 2$ | $21.4 \pm 0.3$ |
| $X^+e^-\bar{\nu}_e, K^0_S\eta$ | $28 \pm 6 \pm 4$ | $7.9 \pm 0.3$ |
| $X^+e^-\bar{\nu}_e, K^0_S\omega$ | $50 \pm 15 \pm 6$ | $8.2 \pm 0.2$ |
| $X^-e^+\nu_e, K^+\pi^-$ | $1218 \pm 47 \pm 17$ | $45.9 \pm 0.2$ |
| $X^-e^+\nu_e, K^-K^+$ | $102 \pm 21 \pm 10$ | $39.0 \pm 0.5$ |
| $X^-e^+\nu_e, \pi^-\pi^+$ | $40 \pm 10 \pm 4$ | $50.5 \pm 0.8$ |
| $X^-e^+\nu_e, K^0_S\pi^0\pi^0$ | $50 \pm 15 \pm 9$ | $9.6 \pm 0.2$ |
| $X^-e^+\nu_e, K^0_S\pi^0$ | $189 \pm 19 \pm 7$ | $21.4 \pm 0.3$ |
| $X^-e^+\nu_e, K^0_S\eta$ | $27 \pm 8 \pm 2$ | $7.7 \pm 0.3$ |
| $X^-e^+\nu_e, K^0_S\omega$ | $49 \pm 16 \pm 4$ | $8.5 \pm 0.2$ |

TABLE VIII: $K^0_L\pi^0$ DT yields and efficiencies with statistical uncertainties input to the data fit.

| Mode | Yield | Efficiency (%) |
|---|---|---|
| $K^0_L\pi^0, K^-\pi^+$ | $187 \pm 14$ | $34.0 \pm 0.2$ |
| $K^0_L\pi^0, K^+\pi^-$ | $179 \pm 14$ | $34.8 \pm 0.2$ |
| $K^0_L\pi^0, K^0_S\pi^0$ | $90 \pm 10$ | $15.5 \pm 0.1$ |
| $K^0_L\pi^0, K^0_S\eta$ | $8.6 \pm 3.1$ | $5.4 \pm 0.1$ |
| $K^0_L\pi^0, K^0_S\omega$ | $34 \pm 6$ | $6.2 \pm 0.1$ |

shows the sources of these measurements, and there is no overlap among the measurements in these Tables.

### A. External Branching Ratio Measurements

Because our precision on $\cos\delta$ is currently limited by our knowledge of the $CP$-eigenstate branching fractions, we include as many external measurements of these branching fractions as possible. Except for the inclusive $\mathcal{B}(K^0_S\pi^0\pi^0)$ and $\mathcal{B}(K^0_L\pi^0)$, all $CP$-eigenstates in this analysis have previous branching ratio measurements with respect to other reference modes.

For $K^0_S\pi^0$, $K^0_S\eta$, and $K^0_S\omega$, we make use of the global branching fraction fit performed in Ref. [29]. Because $\mathcal{B}(K^-\pi^+)$ is a free parameter in this fit and in the current analysis, we also include Ref. [29]'s fit result for this mode in order to properly account for the correlations among these branching fractions. We do not use Ref. [25] because this compilation includes a CLEO-c measurement of $\mathcal{B}(K^-\pi^+)$[17], which is correlated with the measurements in this

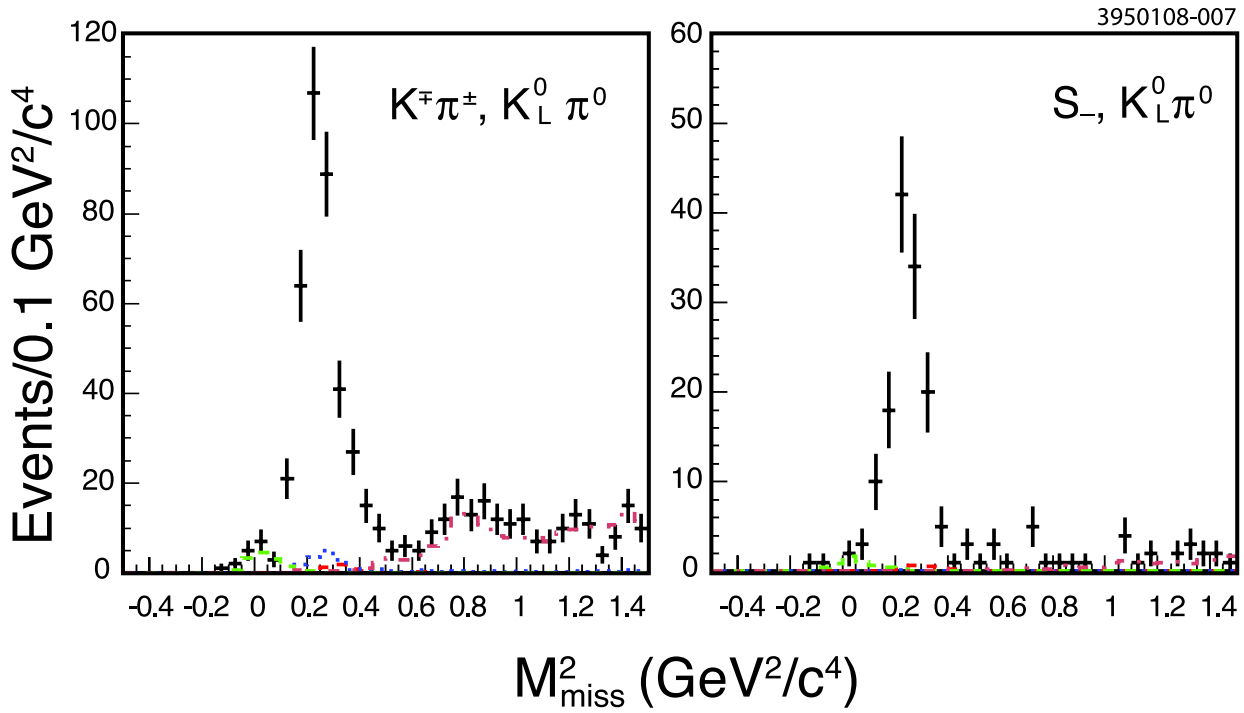


FIG. 5: Sums of $M^2_{\rm miss}$ distributions for $K^0_L\pi^0$. The dashed lines represent simulations of the peaking backgrounds $D^0 \to \pi^0\pi^0$ (dashed), $K^0_S\pi^0$ (dotted), $\eta\pi^0$ (long-dashed), and $K^{*0}\pi^0$ (dot-dashed).

analysis.

Previous experiments have measured $R_{KK} \equiv \mathcal{B}(K^-K^+)/\mathcal{B}(K^-\pi^+)$ and $R_{\pi\pi} \equiv \mathcal{B}(\pi^-\pi^+)/\mathcal{B}(K^-\pi^+)$ simultaneously [25], so these two quantities are correlated both statistically [via the common denominator, $\mathcal{B}(K^-\pi^+)$] and systematically. It is common for these experiments to also report a value of $R_{KK}/R_{\pi\pi}$ in addition to $R_{KK}$ and $R_{\pi\pi}$ separately. Using the dominant measurements of all three quantities [30–33], we compute a weighted average correlation coefficient of 0.30 between the $R_{KK}$ and $R_{\pi\pi}$ values quoted in Ref [25]. For $R_{\pi\pi}$, we remove the CLEO-c measurement [34] from the average because it was based on the same dataset as this analysis.

The CLEO-c $D \to K^0_{S/L}\pi^0$ analysis [28], provides additional information on $\mathcal{B}(K^0_L\pi^0)$ from the $K^-\pi^+\pi^0$ and $K^-\pi^+\pi^-\pi^+$ tag modes, which are not used in this analysis. Systematic correlations between the $K^0_L\pi^0$ yields in this analysis and these additional $\mathcal{B}(K^0_L\pi^0)$ measurements is taken into account. We also include the statistical correlation between $\mathcal{B}(K^0_L\pi^0)$ and $\mathcal{B}(K^0_S\pi^0)$; knowledge of the latter is required to correct for the effect of quantum correlations in the former.

Table X summarizes the external branching fraction inputs to the fit.

TABLE IX: Crossfeed probabilities and peaking background efficiencies and branching fractions input to the fit. Backgrounds marked by an asterisk (*) occur in only in STs, not DTs.

| Crossfeed → Signal | | Efficiency (%) |
|---|---|---|
| $K^+\pi^-$ | $\to K^-\pi^+$ | $0.098 \pm 0.005$ |
| $K^-\pi^+$ | $\to K^+\pi^-$ | $0.092 \pm 0.003$ |
| $K^0_S\omega$ | $\to K^0_S\pi^0\pi^0$ | $0.048 \pm 0.031$ |
| $K^0_S\pi^0$ | $\to K^0_L\pi^0$ | $1.92 \pm 0.03$ |
| **Background → Signal** | **$\mathcal{B}_{\rm bkg}$ (%) [25]** | **Efficiency (%)** |
| $K^0_S\pi^+\pi^-$ | $\to K^0_S\pi^0\pi^0$ | $2.90 \pm 0.19$ | $0.006 \pm 0.012$ |
| $\pi^+\pi^-\pi^0\pi^0$ | $\to K^0_S\pi^0\pi^0$ | $0.98 \pm 0.09$ | $0.029 \pm 0.067$ |
| $K^-\pi^+\pi^0$ (*) | $\to K^0_S\pi^0\pi^0$ | $14.1 \pm 0.5$ | $0.0012 \pm 0.0024$ |
| $D^+ \to K^0_S\pi^+\pi^0$ (*) | $\to K^0_S\pi^0\pi^0$ | $7.22 \pm 0.26$ | $0.048 \pm 0.007$ |
| $\rho^+\pi^-$ | $\to K^0_S\pi^0$ | $1.00 \pm 0.06$ | $0.071 \pm 0.005$ |
| $\rho^0\pi^0$ | $\to K^0_S\pi^0$ | $0.32 \pm 0.04$ | $0.032 \pm 0.033$ |
| Generic $D^0\bar{D}^0$ (*) | $\to K^0_S\pi^0$ | — | $0.00051 \pm 0.00016$ |
| Generic $D^+D^-$ (*) | $\to K^0_S\pi^0$ | — | $0.00038 \pm 0.00012$ |
| $\bar{K}^{*0}\pi^+\pi^-$ | $\to K^0_S\omega$ | $2.3 \pm 0.5$ | $0.065 \pm 0.002$ |
| $K^{*-}\pi^+\pi^0$ | $\to K^0_S\omega$ | $1.00 \pm 0.22$ | $0.135 \pm 0.003$ |
| $K^{*-}\rho^+$ | $\to K^0_S\omega$ | $6.4 \pm 2.5$ | $0.035 \pm 0.001$ |
| $\bar{K}^{*0}\rho^0$ | $\to K^0_S\omega$ | $1.50 \pm 0.33$ | $0.022 \pm 0.004$ |
| $K^0_S\pi^+\pi^-\pi^0$ | $\to K^0_S\omega$ | $1.1 \pm 1.1$ | $0.405 \pm 0.423$ |
| $\pi^+\pi^-\pi^+\pi^-\pi^0$ | $\to K^0_S\omega$ | $0.41 \pm 0.05$ | $0.006 \pm 0.003$ |
| $K_1^-\pi^+$ | $\to K^0_S\omega$ | $1.12 \pm 0.31$ | $0.038 \pm 0.005$ |
| $\bar{K}_1^0\pi^0$ | $\to K^0_S\omega$ | $0.59 \pm 0.02$ | $0.030 \pm 0.010$ |
| $\eta\pi^0$ | $\to K^0_L\pi^0$ | $0.056 \pm 0.014$ | $0.155 \pm 0.001$ |
| $\pi^0\pi^0$ | $\to K^0_L\pi^0$ | $0.079 \pm 0.008$ | $0.117 \pm 0.001$ |

### B. External Mixing Measurements

#### 1. *Information on $r^2$ From Wrong-Sign $D^0 \to K^+\pi^-$ and $D^0 \to K^{(*)+}\ell^-\nu_\ell$*

Studies of wrong-sign $D^0 \to K^+\pi^-$ from other experiments provide information on $r^2$, $y'$, and $R_{\rm M}$. Without using $D^0$ decay times, these analyses are sensitive to the time-integrated wrong-sign rate ratio:

$$R_{\rm WS} \equiv \frac{\Gamma(D^0 \to K^+\pi^-)}{\Gamma(\bar{D}^0 \to K^+\pi^-)} \tag{16}$$

$$= r^2 + ry' + R_{\rm M} \tag{17}$$

$$= r^2 + \sqrt{r^2}y\cos\delta - \sqrt{r^2}x\sin\delta + \frac{x^2+y^2}{2}, \tag{18}$$

where Eq. (18) explicitly shows the dependence on the fit parameters $r^2$, $y$, $\cos\delta$, $x^2$, and $x\sin\delta$. By also measuring the decay times of the same $D^0$ candidates, these experiments can

TABLE X: External branching ratio measurements and their correlations used in the data fit. An asterisk (*) indicates removal of overlapping CLEO-c measurements.

| Parameter | Value (%) | Correlation Coefficients | | | | | |
|---|---|---|---|---|---|---|---|
| $\mathcal{B}(K^-\pi^+)$ | $3.81 \pm 0.09$ [29] | 1 | 0.08 | 0.06 | 0.04 | −0.08 | 0 | 0 |
| $\mathcal{B}(K^0_S\pi^0)$ | $1.15 \pm 0.12$ [29] | | 1 | 0.58 | 0.14 | −0.95 | 0 | 0 |
| $\mathcal{B}(K^0_S\eta)$ | $0.380 \pm 0.060$ [29] | | | 1 | 0.10 | −0.55 | 0 | 0 |
| $\mathcal{B}(K^0_S\omega)$ | $1.30 \pm 0.30$ [29] | | | | 1 | −0.13 | 0 | 0 |
| $\mathcal{B}(K^0_L\pi^0)$ | $1.003 \pm 0.083$* [28] | | | | | 1 | 0 | 0 |
| $\mathcal{B}(K^-K^+)/\mathcal{B}(K^-\pi^+)$ | $10.10 \pm 0.16$ [25] | | | | | | 1 | 0.30 |
| $\mathcal{B}(\pi^-\pi^+)/\mathcal{B}(K^-\pi^+)$ | $3.588 \pm 0.057$* [25] | | | | | | | 1 |

separate the three terms in Eq. (17) because each has a different proper time dependence:

$$\frac{dN}{dt} \propto e^{\Gamma t}\left[r^2 + ry'\Gamma t + \frac{x'^2 + y'^2}{4}(\Gamma t)^2\right]. \tag{19}$$

We use time-integrated $R_{\rm WS}$ measurements as a source of information on $r^2$, which is otherwise poorly determined in our analysis. Constraining $r^2$ leads directly to improved precision on $\cos\delta$ because it always appears as $r\cos\delta$ in Table I. Extracting meaningful precision on $r^2$ from $R_{\rm WS}$ requires information on $x\sin\delta$ and $x^2$. When the external $y$ and $y'$ measurements described in Section IV B 2 are not included in the fit, $x\sin\delta$ is poorly determined, so we take $x\sin\delta$ to be zero. For $x^2$, which is also poorly determined in our analysis, we use $R_{\rm M}$ measurements from wrong-sign $D^0 \to K^{(*)+}\ell^-\nu_\ell$ rates. Table XI shows the input $R_{\rm WS}$ and semileptonic $R_{\rm M}$ measurements, which are uncorrelated with all other measurements and are entered directly into the fit.

TABLE XI: External mixing measurements used to constrain $r^2$.

| Parameter | Average (%) |
|---|---|
| $R_{\rm WS}$ | $0.409 \pm 0.022$ [35–37] |
| $R_{\rm M}$ | $0.0173 \pm 0.0387$ [38–41] |

*2. Measurements of $y$ and $y'$*

By combining external measurements of $y$ and $y'$ with the CLEO-c measurement of $\cos\delta$, the fitter can extract $x\sin\delta$ via $x\sin\delta = y\cos\delta - y'$. In doing so, it accounts for the fact that $y'$ is determined simultaneously with $r^2$ and $R_{\rm M}$, which are also functions of the fit parameters, and that $\cos\delta$ and its uncertainty are correlated with $y$ (as discussed below in Section VI).

External measurements of $y$ come from two sources: comparison of $D^0$ decay times to $CP$ eigenstates $K^+K^-$ and $\pi^+\pi^-$ with decay times to the flavor eigenstate $K^-\pi^+$, and time-dependent Dalitz plot analysis of $D \to K^0_S\pi^+\pi^-$, which is sensitive to both $x$ and $y$.

The latter $x$ and $y$ measurements are essentially uncorrelated, but $x$ provides information on $y$ when combined with measurements of $R_{\rm M}$.

For $y'$, we use three sets of ($CP$-conserving) fit results from CLEO, Belle, and BABAR. Averages of these fits are shown in Table XII. The fit covariance matrices have been provided by the above collaborations and are also included in our analysis.

TABLE XII: External measurements of $y$ and $y'$ with associated measurements of $r^2$ and $x'^2$.

| Parameter | Value (%) |
|---|---|
| $y$ | $0.662 \pm 0.211$ [3, 31, 42–47] |
| $x$ | $0.811 \pm 0.334$ [3, 47] |
| $r^2$ | $0.339 \pm 0.012$ [1, 4, 48] |
| $y'$ | $0.34 \pm 0.30$ [1, 4, 48] |
| $x'^2$ | $0.006 \pm 0.018$ [1, 4, 48] |

We note that, if we assume $x \sin\delta = 0$, the $y$ and $y'$ measurements in Table XII by themselves provide an independent measurement of $\cos\delta = (y' + x\sin\delta)/y = 0.52 \pm 0.49$, which is consistent with but less precise than the value found independently with CLEO-c data (see Section VI).

## V. SYSTEMATIC UNCERTAINTIES

All uncertainties except statistical uncertainties on the input yields are considered systematic in origin. Systematic uncertainties on the fit inputs are included directly in the covariance matrix given to the fitter, which propagates them to the fit parameters. Uncorrelated yield uncertainties are discussed above in Section III. Below, we summarize the sources of correlated uncertainty and the measurements to which they apply.

Final-state-dependent correlated systematic uncertainties, such as for tracking, particle identification (PID), and $\pi^0$ and $K^0_S$ finding efficiencies are the dominant uncertainties for the branching fractions, but, as discussed in Ref. [16], when no external measurements are included, they cancel in the DCS and mixing parameters. However, external measurements are, in general, not subject to the same correlated effects as our input yields. Thus, while these external measurements reduce the statistical uncertainties on $y$ and $\cos\delta$, they also introduce sensitivity to correlated uncertainties, and they increase the systematic uncertainties somewhat.

In Table XIII, we list the correlated systematic uncertainties on reconstruction and PID efficiencies for final state particles, determined as Refs. [24, 49] describe. We also apply the efficiency corrections given in Refs. [24, 49] with the following modifications. For $\pi^0$ finding efficiency, we adjust the relative correction to $-3.3\%$ and inflate the systematic uncertainty to 4.0% to account for our inclusion of signal modes with more energetic $\pi^0$s than in Ref. [24]. For $\eta$ finding efficiency, the relative correction appropriate for our selection criteria is $-6.5\%$ with an uncertainty of 4.0%. For $K^0_S$ finding efficiency, we include additional contributions of 0.3% and 0.4% for the flight significance and invariant mass requirements. We also include uncertainties on peaking background branching fractions, shown in Table IX. The signal and background efficiencies listed in this paper include the corrections discussed above.

Table XIV shows mode-dependent uncertainties. Most are assessed by relaxing selection requirements and noting the resultant change in efficiency-corrected yield. The effect of modeling of the $K^0_S\pi^0\pi^0$ resonant substructure on the efficiency is determined by reweighting the simulated events according to the substructure observed in data and recomputing the efficiency. We assign a conservative uncertainty for the modeling of multiple candidates by taking the difference between multiple candidate rates in simulated events and data. The efficiency of the extra track, $\pi^0$, and $\eta$ vetos in $K^0_L\pi^0$ modes is studied by comparing the frequency of these extra particles between simulated events and data. For semileptonic decays, we extrapolate the observed electron momentum spectrum below 200 MeV/$c$ based on the simulation, and we take 25% of the fraction below this momentum as an associated uncertainty.

In our simulation, final state radiation (FSR) is generated by PHOTOS [50]. We measure efficiencies with and without FSR generation and assign 30% of the difference as a systematic uncertainty. We also include a contribution corresponding to the change in efficiency when PHOTOS does and does not model interference among the radiated photons.

Unlike FSR, initial state radiation (ISR) coherently shifts both $M$ values upward in a signal DT. So, mismodeling of ISR would affect ST and DT efficiencies by the same fraction. Based on a study of excluding events in the ISR region ($M > 1.87$ GeV/$c^2$), we assign a conservative 0.5% uncertainty to all yields.

TABLE XIII: Correlated, fractional efficiency systematic uncertainties and the schemes for applying them in the data branching fraction fit.

| Source | Uncertainty (%) | Scheme |
|---|---|---|
| Track finding | 0.3 | per track |
| $K^\pm$ hadronic interactions | 0.6 | per $K^\pm$ |
| $K^0_S$ finding | 1.9 | per $K^0_S$ |
| $\pi^0$ finding | 4.0 | per $\pi^0$ |
| $\eta$ finding | 4.0 | per $\eta$ |
| $dE/dx$ and RICH | 0.3 | per $\pi^\pm$ PID cut |
| $dE/dx$ and RICH | 0.3 | per $K^\pm$ PID cut |
| EID | 1.0 | per $e^\pm$ |

## VI. FIT RESULTS

We tested the analysis technique with the full simulated sample of uncorrelated $D^0\bar{D}^0$ decays that was reweighted to mimic the effect of quantum correlations. This reweighting leaves a 40% subset with an effective luminosity 15 times that of the data sample. The fit results showed satisfactory agreement with the input values, even when accounting for the statistical correlation between the signal efficiencies (measured in the full sample) and the signal yields (measured in the 40% subset).

In Table XV, we show the results of the standard data fit, which includes external inputs from Tables X and XI. The correlation matrix for this fit is shown in Table XVI. In this fit, we assume $x\sin\delta = 0$, and the associated systematic uncertainty is $\pm 0.03$ for $\cos\delta$ and negligible for all other parameters. We obtain a first measurement of $\cos\delta$, consistent with

TABLE XIV: Correlated, mode-dependent fractional systematic uncertainties in percent for STs. An asterisk (*) marks those uncertainties that are correlated among modes. The schemes by which these uncertainties are applied to DTs are also given, along with the fractional DT uncertainty, $\lambda_{\rm DT}$, on mode $\{A, B\}$ for ST uncertainties of $\alpha$ on mode $A$ and $\beta$ on mode $B$.

| | $\Delta E$ | ISR* | FSR* | Lepton Veto* | Other | |
|---|---|---|---|---|---|---|
| $K^{\mp}\pi^{\pm}$ | 0.5 | 0.5 | 1.2 | 0.5 | | |
| $K^+K^-$ | 0.9 | 0.5 | 0.8 | 0.4 | 0.5 | $K^{\pm}$ $\cos\theta$ cut |
| $\pi^+\pi^-$ | 1.9 | 0.5 | 1.7 | 3.2 | | |
| $K^0_S\pi^0\pi^0$ | 2.6 | 0.5 | | | 1.5 | $K^0_S$ daughter PID |
| | | | | | 0.7 | resonant substructure |
| $K^0_S\pi^0$ | 0.9 | 0.5 | | | | |
| $K^0_S\eta$ | 5.5 | 0.5 | | | 0.3 | $\eta$ mass cut |
| | | | | | 0.7 | $\mathcal{B}(\eta\to\gamma\gamma)$ [25] |
| $K^0_S\omega$ | 1.2 | 0.5 | 0.8 | | 1.4 | $\omega$ mass cut |
| | | | | | 0.8 | $\mathcal{B}(\omega\to\pi^+\pi^-\pi^0)$ [25] |
| $Xe\nu_e$ | | 0.5 | 0.3 | | 2.0 | spectrum extrapolation |
| | | | | | 0.7 | multiple $e^{\pm}$ candidates |
| $K^0_L\pi^0$ | | 0.5 | | | 0.7 | background subtraction |
| | | | | | 0.3 | extra track veto |
| | | | | | 1.4 | signal shape |
| | | | | | 1.6 | extra $\pi^0$ veto |
| | | | | | 0.5 | $\eta$ veto |
| Scheme | per $D$ | per yield | per $D$ | per ST | per $D$ | |
| $\lambda_{\rm DT}$ | $\sqrt{\alpha^2+\beta^2}$ | $(\alpha+\beta)/2$ | $\alpha+\beta$ | 0 | $\sqrt{\alpha^2+\beta^2}$ | |

being at the boundary of the physical region. Our value of $y$ is consistent with the world average of $0.00662\pm0.00211$ (see Table XII). Our branching fraction results do not supersede other CLEO-c measurements.

The likelihood curve for $\cos\delta$ is obtained by repeating this fit at fixed values of $\cos\delta$ and recording the change in optimized $\chi^2$. We then compute $\mathcal{L} = e^{-(\chi^2-\chi^2_{\rm min})/2}$, which is shown in Fig. 6a. It is highly non-Gaussian, so we assign asymmetric uncertainties by finding the values of $\cos\delta$ where $\Delta\chi^2 = 1$ to obtain $\cos\delta = 1.03^{+0.31}_{-0.17} \pm 0.06$. For values of $|\cos\delta| < 1$, we also compute $\mathcal{L}$ as a function of $|\delta|$, and we integrate these curves within the physical region to obtain 95% confidence level limits of $\cos\delta > 0.07$ and $|\delta| < 75^\circ$.

The asymmetric uncertainties on $\cos\delta$ quoted above still do not fully capture the non-linearity of the likelihood. This non-linearity stems from the use of $r^2$ to convert $r\cos\delta$ into $\cos\delta$, which causes the uncertainty on $\cos\delta$ to scale roughly like $1/r$. Because $r^2$ is obtained from $R_{\rm WS}$ via Eq. (18), an upward shift in $y$ lowers the derived value of $r^2$ (for positive $r\cos\delta$). As a result, the uncertainty on $\cos\delta$ increases with more positive $y$, as shown in Fig. 6b. A second, smaller effect is that the sign of the correlation between $r^2$ and $r\cos\delta$ is given by the sign of $y$. When $y$ is positive, $r^2$ and $r\cos\delta$ are anti-correlated, which tends to inflate the uncertainty on $\cos\delta$.

We also perform an extended fit that determines $x\sin\delta$ by including previous measurements of $y$ and $y'$. Table XV shows the results of this fit, which incorporates all external

TABLE XV: Results from the standard fit (with inputs from Tables X and XI) and the extended fit (with inputs from Tables X, XI, and XII). Uncertainties are statistical and systematic, respectively. Charge-averaged $D^0$ branching fractions are denoted by final state.

| Parameter | Standard Fit | Extended Fit |
|---|---|---|
| $\mathcal{N}$ $(10^6)$ | $1.042 \pm 0.021 \pm 0.010$ | $1.042 \pm 0.021 \pm 0.010$ |
| $y$ $(10^{-3})$ | $-45 \pm 59 \pm 15$ | $6.5 \pm 0.2 \pm 2.1$ |
| $r^2$ $(10^{-3})$ | $8.0 \pm 6.8 \pm 1.9$ | $3.44 \pm 0.01 \pm 0.09$ |
| $\cos\delta$ | $1.03 \pm 0.19 \pm 0.06$ | $1.10 \pm 0.35 \pm 0.07$ |
| $x^2$ $(10^{-3})$ | $-1.5 \pm 3.6 \pm 4.2$ | $0.06 \pm 0.01 \pm 0.05$ |
| $x\sin\delta$ $(10^{-3})$ | 0 (fixed) | $4.4 \pm 2.4 \pm 2.9$ |
| $K^-\pi^+$ (%) | $3.78 \pm 0.05 \pm 0.05$ | $3.78 \pm 0.05 \pm 0.05$ |
| $K^-K^+$ $(10^{-3})$ | $3.87 \pm 0.06 \pm 0.06$ | $3.88 \pm 0.06 \pm 0.06$ |
| $\pi^-\pi^+$ $(10^{-3})$ | $1.36 \pm 0.02 \pm 0.03$ | $1.36 \pm 0.02 \pm 0.03$ |
| $K^0_S\pi^0\pi^0$ $(10^{-3})$ | $8.34 \pm 0.45 \pm 0.42$ | $8.35 \pm 0.44 \pm 0.42$ |
| $K^0_S\pi^0$ (%) | $1.14 \pm 0.03 \pm 0.03$ | $1.14 \pm 0.03 \pm 0.03$ |
| $K^0_S\eta$ $(10^{-3})$ | $4.42 \pm 0.15 \pm 0.28$ | $4.42 \pm 0.15 \pm 0.28$ |
| $K^0_S\omega$ (%) | $1.12 \pm 0.04 \pm 0.05$ | $1.12 \pm 0.04 \pm 0.05$ |
| $X^-e^+\nu_e$ (%) | $6.54 \pm 0.17 \pm 0.17$ | $6.59 \pm 0.16 \pm 0.16$ |
| $K^0_L\pi^0$ (%) | $1.01 \pm 0.03 \pm 0.02$ | $1.01 \pm 0.03 \pm 0.02$ |
| $\chi^2_{\rm fit}$/ndof | 30.1/46 | 55.3/57 |

measurements, from Tables X, XI, and XII. The correlation matrix for the extended fit is given in Table XVII. The resultant value of $y$ includes the CLEO-c measurement from the standard fit, but the precision is dominated by the external $y$ measurements. The overall uncertainty on $\cos\delta$ increases to $\pm 0.36$ because of the $R_{\rm WS}$ measurement, as discussed above. However, unlike the standard fit, the likelihood for $\cos\delta$ shown in Fig. 7a is nearly Gaussian. For $x\sin\delta$, we assign asymmetric uncertainties resulting in $x\sin\delta = (4.4^{+2.7}_{-1.8}\pm 2.9)\times 10^{-3}$. By repeating the fit at various simultaneously fixed values of $\cos\delta$ and $\sin\delta$, we also determine $\delta = (22^{+11+9}_{-12-11})^\circ$. The corresponding 95% confidence level intervals within the physical region are $\cos\delta > 0.39$, $x\sin\delta \in [0.002, 0.014]$, and $\delta \in [-7^\circ, +61^\circ]$. Performing this extended fit with $y$, $x^2$, and $x\sin\delta$ fixed to zero results in a change in $\chi^2$ of 25.1, or a significance of $5.0\sigma$.

In the standard fit, the large correlation between $y$ and $r^2$ originates in the use of the $R_{\rm WS}$ measurement in Table XI to provide information on $r^2$. Using Eq. (18), one sees that the precision on $r^2$ is driven by the precision on $y$. Hence, for positive $r\cos\delta$, $r^2$ and $y$ are negatively correlated. Consequently, the $\cos\delta$ value obtained by dividing $r\cos\delta$ by $\sqrt{r^2}$ is positively correlated with $y$. In the extended fit, these correlations are broken by the precise external measurements of $y$ in Table XII, and the weak negative correlation between $\cos\delta$ and $y$ results from Eqs. (10) and (11).

We assess the fit's sensitivity to the assumed quantum correlation parameters in the peaking background subtractions by varying these parameters over their full allowed ranges. We find excursions of less than $1 \times 10^{-4}$ in $y$ and 0.003 in $\cos\delta$ for both the standard and extended fits. We assign a systematic uncertainty, included in Table XV given by the size of these shifts.

TABLE XVI: Correlation coefficients (%) for the standard fit in Table XV using both statistical and systematic uncertainties.

| | $y$ | $r^2$ | $\cos\delta$ | $x^2$ | $K^-\pi^+$ | $K^-K^+$ | $\pi^-\pi^+$ | $K^0_S\pi^0\pi^0$ | $K^0_S\pi^0$ | $K^0_S\eta$ | $K^0_S\omega$ | $X^-e^+\nu_e$ | $K^0_L\pi^0$ |
|---|---|---|---|---|---|---|---|---|---|---|---|---|---|
| $\mathcal{N}$ | −11 | 8 | −22 | −10 | −65 | −61 | −53 | −15 | −42 | −24 | −23 | 2 | 33 |
| $y$ | | −99 | 49 | 99 | −20 | 10 | 6 | −0 | −6 | 1 | −4 | 30 | 7 |
| $r^2$ | | | −38 | −99 | 21 | −8 | −5 | 3 | 9 | 0 | 6 | −30 | −11 |
| $\cos\delta$ | | | | 50 | 2 | 15 | 12 | 17 | 22 | 8 | 13 | 13 | −22 |
| $x^2$ | | | | | −20 | 10 | 6 | −0 | −6 | 1 | −4 | 30 | 7 |
| $K^-\pi^+$ | | | | | | 80 | 77 | 12 | 35 | 19 | 28 | −5 | −28 |
| $K^-K^+$ | | | | | | | 74 | 11 | 30 | 19 | 28 | −6 | −28 |
| $\pi^-\pi^+$ | | | | | | | | 10 | 26 | 15 | 22 | 1 | −21 |
| $K^0_S\pi^0\pi^0$ | | | | | | | | | 64 | 14 | 46 | 0 | −36 |
| $K^0_S\pi^0$ | | | | | | | | | | 29 | 57 | −2 | −65 |
| $K^0_S\eta$ | | | | | | | | | | | 18 | −0 | −21 |
| $K^0_S\omega$ | | | | | | | | | | | | 1 | −36 |
| $X^-e^+\nu_e$ | | | | | | | | | | | | | 2 |

TABLE XVII: Correlation coefficients (%) for the extended fit in Table XV using both statistical and systematic uncertainties.

| | $y$ | $r^2$ | $\cos\delta$ | $x^2$ | $x\sin\delta$ | $K^-\pi^+$ | $K^-K^+$ | $\pi^-\pi^+$ | $K^0_S\pi^0\pi^0$ | $K^0_S\pi^0$ | $K^0_S\eta$ | $K^0_S\omega$ | $X^-e^+\nu_e$ | $K^0_L\pi^0$ |
|---|---|---|---|---|---|---|---|---|---|---|---|---|---|---|
| $\mathcal{N}$ | 0 | −0 | −19 | 0 | −12 | −69 | −61 | −53 | −15 | −43 | −24 | −23 | 5 | 34 |
| $y$ | | 13 | −6 | −6 | 69 | 0 | 0 | −0 | 0 | −0 | −0 | −0 | 1 | 0 |
| $r^2$ | | | −5 | 26 | 37 | −0 | 0 | −0 | 0 | 0 | 0 | 0 | 0 | −0 |
| $\cos\delta$ | | | | −1 | 56 | 14 | 12 | 10 | 20 | 29 | 9 | 17 | 1 | −30 |
| $x^2$ | | | | | 19 | −0 | −0 | −0 | −0 | −0 | −0 | −0 | −0 | 0 |
| $x\sin\delta$ | | | | | | 8 | 8 | 6 | 13 | 18 | 5 | 11 | 1 | −18 |
| $K^-\pi^+$ | | | | | | | 84 | 80 | 12 | 34 | 19 | 28 | 1 | −27 |
| $K^-K^+$ | | | | | | | | 74 | 11 | 31 | 17 | 23 | 1 | −24 |
| $\pi^-\pi^+$ | | | | | | | | | 10 | 27 | 15 | 22 | −0 | −21 |
| $K^0_S\pi^0\pi^0$ | | | | | | | | | | 64 | 14 | 46 | 1 | −36 |
| $K^0_S\pi^0$ | | | | | | | | | | | 29 | 57 | 1 | −65 |
| $K^0_S\eta$ | | | | | | | | | | | | 18 | −0 | −21 |
| $K^0_S\omega$ | | | | | | | | | | | | | 3 | −36 |
| $X^-e^+\nu_e$ | | | | | | | | | | | | | | −1 |

### A. Analysis of Input Information

In this Section, we probe the power of the individual fit inputs or groups of fit inputs by removing them from the standard fit one by one. We define the weight (or information) that each input contributes to fit parameter $\lambda$ to be the fractional change in $1/\sigma^2_\lambda$ when it

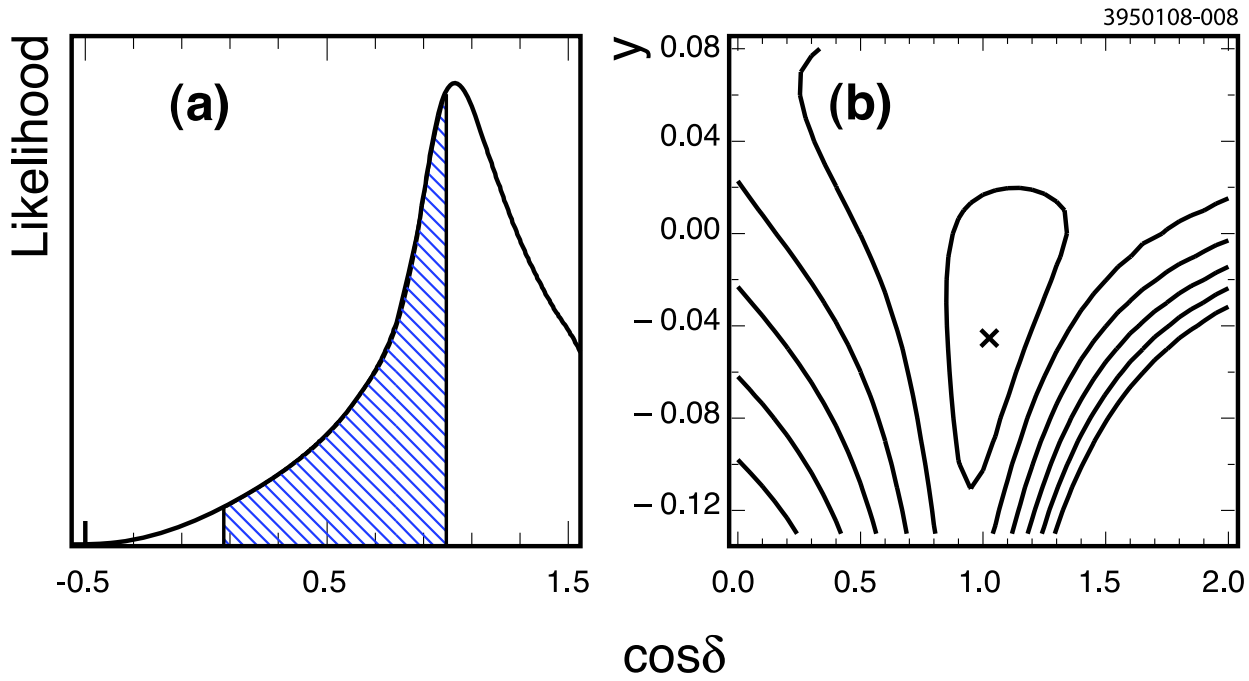


FIG. 6: Standard fit likelihood including both statistical and systematic uncertainties for $\cos\delta$ (a), and simultaneous likelihood for $\cos\delta$ and $y$ (b) shown as contours in increments of $1\sigma$, where $\sigma = \sqrt{\Delta\chi^2}$. The hatched region contains 95% of the area in the physical region.

is removed from the fit:

$$I_\lambda \equiv \frac{1/\sigma_\lambda^2(\text{new}) - 1/\sigma_\lambda^2(\text{standard})}{1/\sigma_\lambda^2(\text{standard})}. \tag{20}$$

Because of the aforementioned non-linearities, removing an input from the fit can result in a $\sigma_\lambda$ that is *smaller* than the standard value, leading to negative $I_\lambda$.

Table XVIII shows $I_\lambda$ for $\lambda = y$ and $\cos\delta$. When $I_\lambda > 0$, we also calculate the significance of the shift to be $\mathcal{S}_\lambda \equiv \Delta\lambda/\sqrt{\sigma_\lambda^2(\text{standard}) - \sigma_\lambda^2(\text{new})}$, where the minus sign accounts for the correlation between the two values of $\lambda$.

As expected from Eqs. (8), (9), and (12), information about $y$ comes primarily from the $\{S_\pm, e\}$ DT yields, which supply 91% of the statistical power. In addition, the $\{K\pi, e\}$ yields provide the normalizing semileptonic branching fraction, and $S_\pm$ ST yields provide $\mathcal{N}\mathcal{B}_{S_\pm}$. Because $y$ is determined from ratios of these quantities, a meaningful measurement depends on the simultaneous presence of various combinations of inputs. For instance, removing the $S_\pm$ ST yields would also reduce the power of the $\{S_\pm, e\}$ DT yields because, then, Eq. (8) cannot be used. Table XVIII does not account for such double-counting of information; it simply shows $I_\lambda$ as each individual input is removed from the fit. For this reason, the sum of all $I_y$ exceeds 100%.

This effect is even more pronounced with $\cos\delta$. As demonstrated in Eqs. (10) and (13), almost all the information about $r\cos\delta$ is contained in the $\{K\pi, S_\pm\}$ DT yields, but only when they are combined with the $\mathcal{B}_{S_\pm}$ estimates provided by the $S_\pm$ ST yields. Furthermore, in order to obtain $\cos\delta$ from $r\cos\delta$, we rely on the inputs from Table XI, which therefore have $I_{\cos\delta} = 1$. If either $\{K\pi, S_+\}$ or $\{K\pi, S_-\}$ yields are removed, then the asymmetries in Eqs. (10) and (13) cannot be formed. However, $r\cos\delta$ can still be obtained with knowledge

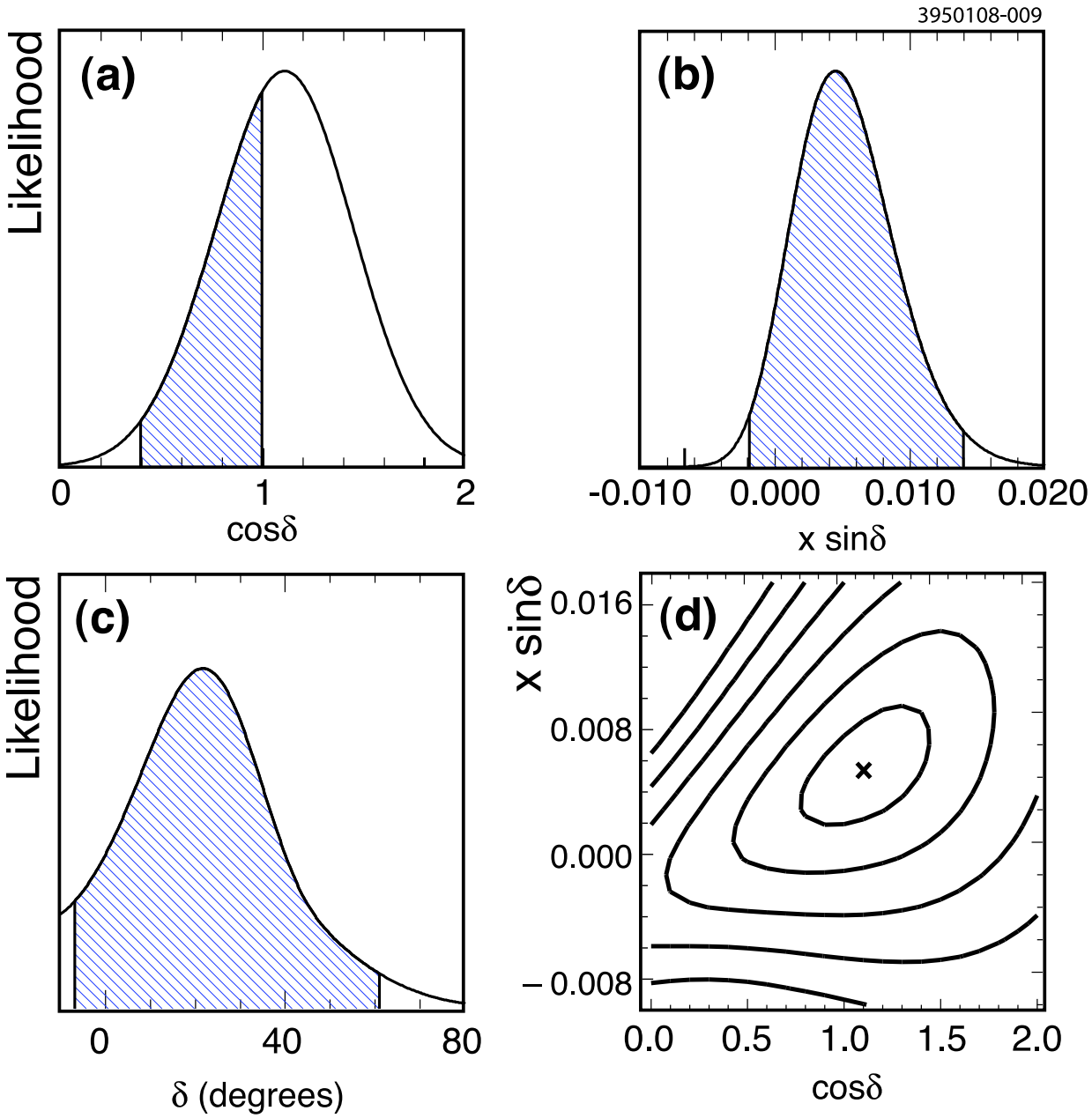


FIG. 7: Extended fit likelihood including both statistical and systematic uncertainties for $\cos\delta$ (a), $x\sin\delta$ (b), $\delta$ (c), and simultaneous likelihood for $\cos\delta$ and $x\sin\delta$ (d) shown as contours in increments of $1\sigma$, where $\sigma = \sqrt{\Delta\chi^2}$. The hatched regions contain 95% of the area in the physical regions. For $\delta$, the fit fails to converge beyond the limits of the plot.

of $\mathcal{N}\mathcal{B}_{K^-\pi^+}\mathcal{B}_{S_\pm}$, which comes from other inputs in the fit.

A striking example of non-linearities in the fit occurs when $\{S_-, e^\pm\}$ double tags are removed. Doing so causes $y$ to fluctuate downward, which, in turn, *lowers* the uncertainty on $\cos\delta$, as discussed above. As a result, $\{S_-, e^\pm\}$ double tags appear to have large *negative* information content.

In performing this exercise, we also test for anomalous inputs that bias the fit results with

undue weight. As Table XVIII shows, we find no evidence of instability from our choice of fit inputs.

TABLE XVIII: Effect of removing inputs from the standard fit. For each input and fit parameter combination, we report the significance of the shift in central value $\mathcal{S}_\lambda$ and the fractional information content $I_\lambda$. In cases where $I_\lambda$ is negative, we do not report the shift significance.

| Removed Input | $\mathcal{S}_y$ | $I_y$ | $\mathcal{S}_{\cos\delta}$ | $I_{\cos\delta}$ |
|---|---|---|---|---|
| Single Tag Yields | | | | |
| $K^-\pi^+$ | $+0.1\sigma$ | 0% | $-0.0\sigma$ | 0% |
| $K^+\pi^-$ | $+0.2\sigma$ | 0% | $-0.0\sigma$ | 1% |
| $K^+K^-$ | $+1.1\sigma$ | 6% | $+0.4\sigma$ | 41% |
| $\pi^+\pi^-$ | $+0.6\sigma$ | 1% | $+0.2\sigma$ | 11% |
| $K^0_S\pi^0\pi^0$ | $+0.5$ | 2% | $+0.4\sigma$ | 23% |
| $K^0_S\pi^0$ | $+1.1\sigma$ | 14% | $+0.5\sigma$ | 72% |
| $K^0_S\eta$ | $-2.8\sigma$ | 0% | — | $-31\%$ |
| $K^0_S\omega$ | $-2.5\sigma$ | 2% | — | $-46\%$ |
| Double Tag Yields | | | | |
| $K^\pm\pi^\mp, K^\pm\pi^\mp$ | $+0.1\sigma$ | 1% | $+0.1\sigma$ | 8% |
| $K^-\pi^+, K^+\pi^-$ | — | $-0\%$ | — | $-2\%$ |
| $K\pi, S_+$ | — | $-0\%$ | $-0.0\sigma$ | 48% |
| $K\pi, S_-$ | $-0.1\sigma$ | 0% | $+0.0\sigma$ | 38% |
| $S_+, S_-$ | $+0.9\sigma$ | 0% | $+0.2\sigma$ | 11% |
| $K\pi, e^\pm$ | $-0.0\sigma$ | 11% | $-0.1\sigma$ | 1% |
| $S'_+, e^\pm$ | $-0.3\sigma$ | 37% | — | $-19\%$ |
| $S_-, e^\pm$ | $-0.9\sigma$ | 54% | — | $-135\%$ |
| $K^0_L\pi^0, K\pi$ | — | $-3\%$ | $-1.3\sigma$ | 14% |
| $K^0_L\pi^0, S_-$ | — | $-0\%$ | $+0.2\sigma$ | 5% |
| External or Other CLEO-c (*) Inputs | | | | |
| $R_{\rm WS}$, $R_{\rm M}$ | $-0.6\sigma$ | 3% | — | 100% |
| $\mathcal{B}(K^-\pi^+)$ | $-1.2\sigma$ | 1% | — | $-12\%$ |
| $\mathcal{B}(K^+K^-)$ | $+1.4\sigma$ | 3% | $+0.2\sigma$ | 29% |
| $\mathcal{B}(\pi^+\pi^-)$ | — | $-0\%$ | — | $-1\%$ |
| $\mathcal{B}(K^0_S\pi^0)$ | $+0.4\sigma$ | 1% | $-0.2\sigma$ | 3% |
| $\mathcal{B}(K^0_S\eta)$ | $+1.4\sigma$ | 0% | $+0.0\sigma$ | 5% |
| $\mathcal{B}(K^0_S\omega)$ | $+0.1\sigma$ | 0% | $-0.3\sigma$ | 0% |
| $\mathcal{B}(K^0_L\pi^0)$* | — | $-5\%$ | $-1.2\sigma$ | 6% |

### B. Purity of *C*-Odd Initial State

The purity of the $C$-odd $D^0\bar{D}^0$ initial state may be diluted by a radiated photon, which would reverse the $C$ eigenvalue of the $D^0\bar{D}^0$ system and thus bias the fit results. ISR, FSR, and bremsstrahlung photon emission are benign because they do not alter the relative angular momentum between the $D^0$ and $\bar{D}^0$, occuring either before the $D^0\bar{D}^0$ are formed

or after they decay. One problematic process would be photon radiation from the $\psi(3770)$, resulting in a virtual $0^+$ state that then decays to $D^0\bar{D}^0$. This channel is suppressed, as there are no nearby $0^+$ states available. Another possible contribution would be $\psi(3770)$ decay to a virtual $D^{*0}\bar{D}^0$, which subsequently decays to $D^0\bar{D}^0\gamma$. Theoretical estimates of these amplitudes indicate a $\psi(3770) \to D^0\bar{D}^0\gamma$ branching fraction of less than $10^{-8}$ [51].

We verify the absence of this effect in data by searching for same-$CP$ DT signals, which would be maximally enhanced for the $C$-even configuration. As shown in Fig. 8 and Table XIX, all such modes have yields consistent with zero. To determine the $C$-even fraction of the $D^0\bar{D}^0$ sample, $\mathcal{N}_{C+}/\mathcal{N}_{C-}$, we perform a variant of the standard and extended fits that include the 15 same-$CP$ DT yields and efficiencies shown in Table XIX. We then express each yield as a sum of $C$-odd and $C$-even contributions: $N_{ij} = \mathcal{N}_{C-}A_i^2A_j^2R_{C-} + \mathcal{N}_{C+}A_i^2A_j^2R_{C+}$, where $R_{C-}$ and $R_{C+}$ are the functions of $y$, $r$, $\cos\delta$, and $x\sin\delta$ given in Table XX. The results of these fits are shown in Table XXI. The $C$-even fraction is found to be consistent with zero, with an uncertainty of 2.4%, and shifts of the fit parameters from the nominal fit results are negligible compared to the systematic uncertainties already assigned.

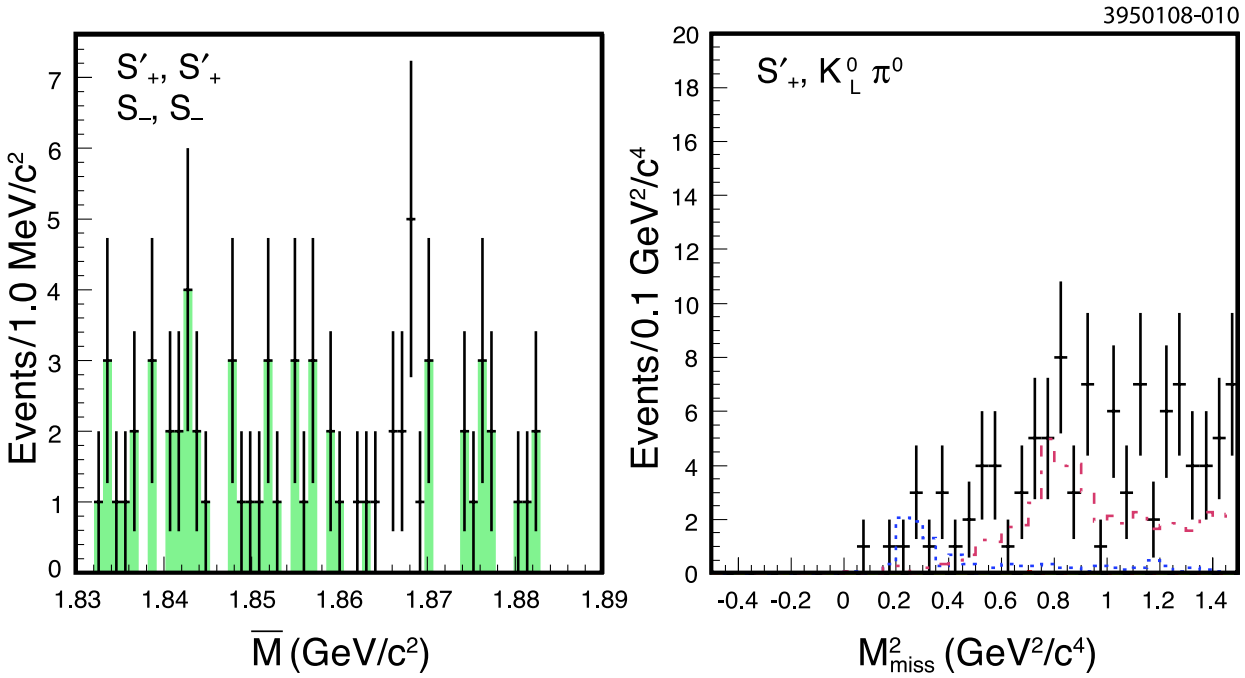


FIG. 8: Combined $\bar{M}$ distribution for fully reconstructed same-$CP$ $\{S'_+, S'_+\}$ and $\{S_-, S_-\}$ DT modes and combined $M^2_{\rm miss}$ distribution for $\{S'_+, K^0_L\pi^0\}$ modes. Data are shown as points with error bars. The shaded histograms show events outside the signal region, and the dashed lines represent simulations of the peaking backgrounds $D^0 \to \pi^0\pi^0$ (dashed), $K^0_S\pi^0$ (dotted), $\eta\pi^0$ (long-dashed), and $K^{*0}\pi^0$ (dot-dashed).

## VII. SUMMARY

We employ a double tagging technique with quantum-correlated $D^0\bar{D}^0$ decays at the $\psi(3770)$ to perform a first measurement of $\cos\delta = 1.03^{+0.31}_{-0.17} \pm 0.06$, where the uncertainties are statistical and systematic, respectively. Within the physical region, we find $|\delta| < 75^\circ$ at

TABLE XIX: Same-$CP$ double tag yields and efficiencies included in the $C$-even-allowed fit.

| Mode | Yield | Efficiency (%) |
|---|---|---|
| $K^+K^-, K^+K^-$ | $-2.1 \pm 1.5 \pm 3.1$ | $32.4 \pm 1.7$ |
| $K^+K^-, \pi^+\pi^-$ | $0.9 \pm 1.6 \pm 1.1$ | $38.9 \pm 2.2$ |
| $K^+K^-, K^0_S\pi^0\pi^0$ | $0.0 \pm 1.0 \pm 0.0$ | $6.6 \pm 0.5$ |
| $\pi^+\pi^-, \pi^+\pi^-$ | $1.2 \pm 2.8 \pm 4.8$ | $44.9 \pm 5.1$ |
| $\pi^+\pi^-, K^0_S\pi^0\pi^0$ | $1.0 \pm 1.0 \pm 0.0$ | $9.2 \pm 1.0$ |
| $K^0_S\pi^0\pi^0, K^0_S\pi^0\pi^0$ | $0.0 \pm 1.0 \pm 0.0$ | $1.5 \pm 0.2$ |
| $K^0_S\pi^0, K^0_S\pi^0$ | $0.0 \pm 1.0 \pm 0.0$ | $8.9 \pm 0.5$ |
| $K^0_S\pi^0, K^0_S\eta$ | $0.0 \pm 1.0 \pm 0.0$ | $2.9 \pm 0.3$ |
| $K^0_S\pi^0, K^0_S\omega$ | $1.0 \pm 1.0 \pm 0.0$ | $3.3 \pm 0.2$ |
| $K^0_S\eta, K^0_S\eta$ | $0.0 \pm 1.0 \pm 0.0$ | $0.7 \pm 0.4$ |
| $K^0_S\eta, K^0_S\omega$ | $0.0 \pm 1.0 \pm 0.0$ | $1.0 \pm 0.2$ |
| $K^0_S\omega, K^0_S\omega$ | $1.0 \pm 1.0 \pm 0.0$ | $1.5 \pm 0.2$ |
| $K^0_L\pi^0, K^+K^-$ | $1.7 \pm 2.1 \pm 0.0$ | $28.2 \pm 0.1$ |
| $K^0_L\pi^0, \pi^+\pi^-$ | $4.3 \pm 2.4 \pm 0.0$ | $38.5 \pm 0.1$ |
| $K^0_L\pi^0, K^0_S\pi^0\pi^0$ | $2.7 \pm 2.3 \pm 0.0$ | $6.4 \pm 0.1$ |

TABLE XX: Comparison of $C$-odd and $C$-even yields, normalized by $\mathcal{N}A_i^2$ for ST modes $i$ and by $\mathcal{N}A_i^2A_j^2$ for DT modes $\{i,j\}$, to leading order in $x$, $y$, and $r^2$, with $y' \equiv y\cos\delta - x\sin\delta$ and $\tilde{y} \equiv y\cos\delta + x\sin\delta$. Charge conjugate modes are implied.

| Mode | $R_{C-}$ | $R_{C+}$ |
|---|---|---|
| $K^-\pi^+$ | $1 + 2ry\cos\delta + r^2$ | $1 + 2ry\cos\delta + r^2$ |
| $S_+$ | $2(1-y)$ | $2(1-y)$ |
| $S_-$ | $2(1+y)$ | $2(1+y)$ |
| $K^-\pi^+, K^-\pi^+$ | $R_{\rm M}$ | $2r(r+y')$ |
| $K^-\pi^+, K^+\pi^-$ | $1 + 2r^2(1-2\cos^2\delta)$ | $1 - 2r^2(1-2\cos^2\delta) + 4r\tilde{y}$ |
| $K^-\pi^+, S_+$ | $1 + 2r\cos\delta + r^2$ | $\left[1 - 2r\cos\delta + r^2\right](1-2y)$ |
| $K^-\pi^+, S_-$ | $1 - 2r\cos\delta + r^2$ | $\left[1 + 2r\cos\delta + r^2\right](1+2y)$ |
| $K^-\pi^+, e^-$ | 1 | $1 + 2r\tilde{y}$ |
| $S_+, S_+$ | 0 | $2(1-2y)$ |
| $S_-, S_-$ | 0 | $2(1+2y)$ |
| $S_+, S_-$ | 4 | 0 |
| $S_+, e^-$ | 1 | $1-2y$ |
| $S_-, e^-$ | 1 | $1+2y$ |

the 95% confidence level. By including external inputs on $y$ and $y'$ in the fit, we find an alternative value of $\cos\delta = 1.10 \pm 0.35 \pm 0.07$, as well as $x\sin\delta = (4.4^{+2.7}_{-1.8} \pm 2.9) \times 10^{-3}$ and $\delta = (22^{+11+9}_{-12-11})^\circ$.

TABLE XXI: Results from the fits allowing for a $C$-even component in the initial state, with inputs from Table XIX. Uncertainties are statistical and systematic, respectively. We also give the shifts in the fit results with respect to the nominal fits.

| Parameter | Standard, $C$-even Allowed | Shift | Extended, $C$-even Allowed | Shift |
|---|---|---|---|---|
| $\mathcal{N}_{C-}$ $(10^6)$ | $1.044 \pm 0.029 \pm 0.017$ | $+0.002$ | $1.044 \pm 0.030 \pm 0.017$ | $+0.002$ |
| $\mathcal{N}_{C+}/\mathcal{N}_{C-}$ $(10^{-3})$ | $-1.5 \pm 23.0 \pm 2.2$ | — | $-1.4 \pm 23.6 \pm 1.9$ | — |
| $y$ $(10^{-3})$ | $-46 \pm 59 \pm 16$ | $-0.2$ | $6.5 \pm 0.2 \pm 2.1$ | $-0.0$ |
| $r^2$ $(10^{-3})$ | $8.0 \pm 6.8 \pm 1.9$ | $+0.008$ | $3.44 \pm 0.01 \pm 0.09$ | $-0.000$ |
| $\cos\delta$ | $1.02 \pm 0.19 \pm 0.06$ | $-0.003$ | $1.10 \pm 0.35 \pm 0.07$ | $-0.005$ |
| $x^2$ $(10^{-3})$ | $-1.5 \pm 4.1 \pm 3.8$ | $-0.2$ | $0.06 \pm 0.01 \pm 0.05$ | $+0.01$ |
| $x\sin\delta$ $(10^{-3})$ | 0 (fixed) | — | $4.4 \pm 2.4 \pm 2.9$ | $-0.04$ |
| $\mathcal{B}(K^-\pi^+)$ (%) | $3.78 \pm 0.05 \pm 0.05$ | $-0.001$ | $3.78 \pm 0.05 \pm 0.05$ | $-0.001$ |
| $\mathcal{B}(K^-K^+)$ $(10^{-3})$ | $3.87 \pm 0.06 \pm 0.06$ | $+0.001$ | $3.88 \pm 0.06 \pm 0.06$ | $+0.001$ |
| $\mathcal{B}(\pi^-\pi^+)$ $(10^{-3})$ | $1.36 \pm 0.02 \pm 0.03$ | $-0.000$ | $1.36 \pm 0.02 \pm 0.03$ | $-0.000$ |
| $\mathcal{B}(K^0_S\pi^0\pi^0)$ $(10^{-3})$ | $8.33 \pm 0.45 \pm 0.42$ | $-0.011$ | $8.34 \pm 0.44 \pm 0.42$ | $-0.011$ |
| $\mathcal{B}(K^0_S\pi^0)$ (%) | $1.14 \pm 0.03 \pm 0.03$ | $-0.001$ | $1.14 \pm 0.03 \pm 0.03$ | $-0.001$ |
| $\mathcal{B}(K^0_S\eta)$ $(10^{-3})$ | $4.42 \pm 0.15 \pm 0.28$ | $-0.002$ | $4.41 \pm 0.15 \pm 0.28$ | $-0.002$ |
| $\mathcal{B}(K^0_S\omega)$ (%) | $1.11 \pm 0.04 \pm 0.05$ | $-0.006$ | $1.11 \pm 0.04 \pm 0.05$ | $-0.006$ |
| $\mathcal{B}(X^-e^+\nu_e)$ (%) | $6.54 \pm 0.17 \pm 0.17$ | $-0.001$ | $6.59 \pm 0.16 \pm 0.16$ | $-0.001$ |
| $\mathcal{B}(K^0_L\pi^0)$ (%) | $1.01 \pm 0.03 \pm 0.02$ | $+0.000$ | $1.01 \pm 0.03 \pm 0.02$ | $+0.000$ |
| $\chi^2_{\rm fit}$/ndof | 34.1/59 | | 59.3/71 | |


### Acknowledgments

We thank Alexey Petrov, William Lockman, Alan Schwartz, Bostjan Golob, and Brian Petersen for helpful discussions. We gratefully acknowledge the effort of the CESR staff in providing us with excellent luminosity and running conditions. D. Cronin-Hennessy and A. Ryd thank the A.P. Sloan Foundation. This work was supported by the National Science Foundation, the U.S. Department of Energy, and the Natural Sciences and Engineering Research Council of Canada.


## APPENDIX A: CORRECTED YIELDS

For use by future experiments, we provide our efficiency-corrected, background-subtracted yields in Tables XXII and XXIII. The correlation matrix, including statistical and systematic uncertainties, for these yields appears in Tables XXIV–XXIX.

## APPENDIX B: FIT RESULTS WITHOUT EXTERNAL MIXING PARAMETER INPUTS

Other charm mixing analyses may wish to include our results without any external mixing parameter inputs. Therefore, we perform a variation on the standard fit in Table XV that uses branching fractions from Table X, but not the external $R_{\rm WS}$ and $R_{\rm M}$ measurements in

TABLE XXII: Efficiency-corrected, background-subtracted single tag and double tag yields input to the fits. Uncertainties are statistical and systematic combined.

| Mode | Yield |
|---|---|
| $K^-\pi^+$ | $39159 \pm 743$ |
| $K^+\pi^-$ | $39326 \pm 742$ |
| $K^+K^-$ | $8279 \pm 208$ |
| $\pi^+\pi^-$ | $2877 \pm 145$ |
| $K^0_S\pi^0\pi^0$ | $18759 \pm 1731$ |
| $K^0_S\pi^0$ | $24923 \pm 1167$ |
| $K^0_S\eta$ | $10078 \pm 790$ |
| $K^0_S\omega$ | $23903 \pm 1581$ |
| $K^-\pi^+, K^-\pi^+$ | $3.1 \pm 3.9$ |
| $K^-\pi^+, K^+\pi^-$ | $1460 \pm 78$ |
| $K^-\pi^+, K^+K^-$ | $199 \pm 25$ |
| $K^-\pi^+, \pi^+\pi^-$ | $53 \pm 11$ |
| $K^-\pi^+, K^0_S\pi^0\pi^0$ | $393 \pm 79$ |
| $K^-\pi^+, K^0_S\pi^0$ | $472 \pm 55$ |
| $K^-\pi^+, K^0_S\eta$ | $131 \pm 49$ |
| $K^-\pi^+, K^0_S\omega$ | $337 \pm 76$ |
| $K^+\pi^-, K^+\pi^-$ | $2.6 \pm 3.2$ |
| $K^+\pi^-, K^+K^-$ | $149 \pm 21$ |
| $K^+\pi^-, \pi^+\pi^-$ | $53 \pm 11$ |
| $K^+\pi^-, K^0_S\pi^0\pi^0$ | $409 \pm 80$ |
| $K^+\pi^-, K^0_S\pi^0$ | $401 \pm 51$ |
| $K^+\pi^-, K^0_S\eta$ | $145 \pm 50$ |
| $K^+\pi^-, K^0_S\omega$ | $370 \pm 77$ |
| $K^+K^-, K^+K^-$ | $-6.5 \pm 10.6$ |
| $K^+K^-, \pi^+\pi^-$ | $2.3 \pm 5.0$ |
| $K^+K^-, K^0_S\pi^0\pi^0$ | $-0.3 \pm 15.0$ |
| $K^+K^-, K^0_S\pi^0$ | $224 \pm 38$ |
| $K^+K^-, K^0_S\eta$ | $97 \pm 38$ |
| $K^+K^-, K^0_S\omega$ | $285 \pm 67$ |
| $\pi^+\pi^-, \pi^+\pi^-$ | $2.7 \pm 12.4$ |
| $\pi^+\pi^-, K^0_S\pi^0\pi^0$ | $11 \pm 11$ |
| $\pi^+\pi^-, K^0_S\pi^0$ | $67 \pm 19$ |
| $\pi^+\pi^-, K^0_S\eta$ | $24 \pm 18$ |

Table XI. The results of this fit are shown in Tables XXX and XXXI. Because $r^2$ is negative in this fit, we cannot extract $\cos\delta$; instead, we quote $r\cos\delta$. Also, we fit for $R_{\rm M}$ instead of $x^2$.

TABLE XXIII: Efficiency-corrected, background-subtracted single tag and double tag yields input to the fits. Uncertainties are statistical and systematic combined.

| Mode | Yield |
|---|---|
| $\pi^+\pi^-, K^0_S\omega$ | $67 \pm 27$ |
| $K^0_S\pi^0\pi^0, K^0_S\pi^0\pi^0$ | $-0.7 \pm 65.8$ |
| $K^0_S\pi^0\pi^0, K^0_S\pi^0$ | $395 \pm 121$ |
| $K^0_S\pi^0\pi^0, K^0_S\eta$ | $327 \pm 168$ |
| $K^0_S\pi^0\pi^0, K^0_S\omega$ | $265 \pm 159$ |
| $K^0_S\pi^0, K^0_S\pi^0$ | $-2.5 \pm 11.0$ |
| $K^0_S\pi^0, K^0_S\eta$ | $-1.0 \pm 33.5$ |
| $K^0_S\pi^0, K^0_S\omega$ | $5.7 \pm 31.7$ |
| $K^0_S\eta, K^0_S\eta$ | $0 \pm 141$ |
| $K^0_S\eta, K^0_S\omega$ | $-9.4 \pm 98.1$ |
| $K^0_S\omega, K^0_S\omega$ | $47 \pm 66$ |
| $X^+e^-\bar{\nu}_e, K^-\pi^+$ | $2488 \pm 131$ |
| $X^+e^-\bar{\nu}_e, K^-K^+$ | $319 \pm 62$ |
| $X^+e^-\bar{\nu}_e, \pi^-\pi^+$ | $97 \pm 28$ |
| $X^+e^-\bar{\nu}_e, K^0_S\pi^0\pi^0$ | $418 \pm 289$ |
| $X^+e^-\bar{\nu}_e, K^0_S\pi^0$ | $903 \pm 119$ |
| $X^+e^-\bar{\nu}_e, K^0_S\eta$ | $349 \pm 94$ |
| $X^+e^-\bar{\nu}_e, K^0_S\omega$ | $601 \pm 202$ |
| $X^-e^+\nu_e, K^+\pi^-$ | $2653 \pm 135$ |
| $X^-e^+\nu_e, K^-K^+$ | $261 \pm 60$ |
| $X^-e^+\nu_e, \pi^-\pi^+$ | $79 \pm 22$ |
| $X^-e^+\nu_e, K^0_S\pi^0\pi^0$ | $518 \pm 190$ |
| $X^-e^+\nu_e, K^0_S\pi^0$ | $876 \pm 103$ |
| $X^-e^+\nu_e, K^0_S\eta$ | $349 \pm 110$ |
| $X^-e^+\nu_e, K^0_S\omega$ | $570 \pm 200$ |
| $K^0_L\pi^0, K^-\pi^+$ | $516 \pm 47$ |
| $K^0_L\pi^0, K^+\pi^-$ | $485 \pm 46$ |
| $K^0_L\pi^0, K^+K^-$ | $-6.8 \pm 7.8$ |
| $K^0_L\pi^0, \pi^+\pi^-$ | $7.1 \pm 6.3$ |
| $K^0_L\pi^0, K^0_S\pi^0\pi^0$ | $10 \pm 37$ |
| $K^0_L\pi^0, K^0_S\pi^0$ | $565 \pm 75$ |
| $K^0_L\pi^0, K^0_S\eta$ | $154 \pm 59$ |
| $K^0_L\pi^0, K^0_S\omega$ | $508 \pm 105$ |


[1] L. M. Zhang *et al.* [Belle Collaboration], Phys. Rev. Lett. **96**, 151801 (2006) [arXiv:hep-ex/0601029].

[2] M. Staric *et al.* [Belle Collaboration], Phys. Rev. Lett. **98**, 211803 (2007) [arXiv:hep-ex/0703036].

TABLE XXIV: Correlation coefficients (%), with statistical and systematic uncertainties, for the efficiency-corrected, background-subtracted yields in Tables XXII and XXIII. Coefficients of 100% are represented by a dash (—).

| | $K^-\pi^+$ | $K^+\pi^-$ | $K^+K^-$ | $\pi^+\pi^-$ | $K^0_S\pi^0\pi^0$ | $K^0_S\pi^0$ | $K^0_S\eta$ | $K^0_S\omega$ | $K^-\pi^+, K^-\pi^+$ | $K^-\pi^+, K^+\pi^-$ | $K^-\pi^+, K^+K^-$ | $K^-\pi^+, \pi^+\pi^-$ | $K^-\pi^+, K^0_S\pi^0\pi^0$ | $K^-\pi^+, K^0_S\pi^0$ | $K^-\pi^+, K^0_S\eta$ | $K^-\pi^+, K^0_S\omega$ | $K^+\pi^-, K^+\pi^-$ | $K^+\pi^-, K^+K^-$ | $K^+\pi^-, \pi^+\pi^-$ | $K^+\pi^-, K^0_S\pi^0\pi^0$ | $K^+\pi^-, K^0_S\pi^0$ | $K^+\pi^-, K^0_S\eta$ | $K^+\pi^-, K^0_S\omega$ |
|---|---|---|---|---|---|---|---|---|---|---|---|---|---|---|---|---|---|---|---|---|---|---|---|
| $K^-\pi^+$ | — | 88 | 56 | 46 | 3 | 7 | 4 | 18 | 0 | 58 | 21 | 16 | 9 | 14 | 6 | 15 | −0 | 22 | 16 | 8 | 13 | 5 | 13 |
| $K^+\pi^-$ | | — | 56 | 46 | 3 | 7 | 4 | 18 | −0 | 58 | 19 | 15 | 8 | 12 | 5 | 14 | 1 | 23 | 17 | 9 | 15 | 6 | 14 |
| $K^+K^-$ | | | — | 25 | 2 | 5 | 3 | 10 | 0 | 34 | 24 | 9 | 5 | 8 | 3 | 8 | 0 | 26 | 9 | 5 | 9 | 3 | 8 |
| $\pi^+\pi^-$ | | | | — | 1 | 2 | 1 | 8 | 0 | 20 | 6 | 15 | 3 | 4 | 2 | 6 | 0 | 7 | 16 | 3 | 5 | 2 | 6 |
| $K^0_S\pi^0\pi^0$ | | | | | — | 82 | 5 | 63 | 0 | 2 | 1 | 1 | 43 | 28 | 1 | 22 | 0 | 1 | 1 | 42 | 31 | 1 | 22 |
| $K^0_S\pi^0$ | | | | | | — | 10 | 70 | 0 | 4 | 1 | 1 | 38 | 35 | 3 | 25 | 0 | 2 | 1 | 37 | 38 | 3 | 24 |
| $K^0_S\eta$ | | | | | | | — | 8 | 0 | 2 | 1 | 1 | 2 | 4 | 23 | 3 | 0 | 1 | 1 | 2 | 4 | 22 | 3 |
| $K^0_S\omega$ | | | | | | | | — | 0 | 12 | 4 | 4 | 30 | 26 | 3 | 37 | 0 | 4 | 4 | 30 | 28 | 3 | 36 |
| $K^-\pi^+, K^-\pi^+$ | | | | | | | | | — | −2 | 0 | 0 | 0 | 0 | 0 | 0 | 0 | 0 | 0 | 0 | 0 | 0 | 0 |
| $K^-\pi^+, K^+\pi^-$ | | | | | | | | | | — | 13 | 11 | 5 | 8 | 4 | 9 | −2 | 15 | 11 | 5 | 9 | 3 | 9 |
| $K^-\pi^+, K^+K^-$ | | | | | | | | | | | — | 4 | 2 | 3 | 1 | 3 | 0 | 6 | 4 | 2 | 3 | 1 | 3 |
| $K^-\pi^+, \pi^+\pi^-$ | | | | | | | | | | | | — | 2 | 2 | 1 | 3 | 0 | 4 | 4 | 2 | 3 | 1 | 3 |
| $K^-\pi^+, K^0_S\pi^0\pi^0$ | | | | | | | | | | | | | — | 14 | 1 | 11 | 0 | 2 | 2 | 19 | 15 | 1 | 11 |
| $K^-\pi^+, K^0_S\pi^0$ | | | | | | | | | | | | | | — | 2 | 10 | 0 | 3 | 2 | 14 | 14 | 2 | 10 |
| $K^-\pi^+, K^0_S\eta$ | | | | | | | | | | | | | | | — | 2 | 0 | 1 | 1 | 1 | 2 | 5 | 2 |
| $K^-\pi^+, K^0_S\omega$ | | | | | | | | | | | | | | | | — | 0 | 4 | 3 | 11 | 11 | 2 | 13 |
| $K^+\pi^-, K^+\pi^-$ | | | | | | | | | | | | | | | | | — | 0 | 0 | 0 | 0 | 0 | 0 |
| $K^+\pi^-, K^+K^-$ | | | | | | | | | | | | | | | | | | — | 4 | 2 | 4 | 1 | 4 |
| $K^+\pi^-, \pi^+\pi^-$ | | | | | | | | | | | | | | | | | | | — | 2 | 3 | 1 | 3 |
| $K^+\pi^-, K^0_S\pi^0\pi^0$ | | | | | | | | | | | | | | | | | | | | — | 15 | 1 | 11 |
| $K^+\pi^-, K^0_S\pi^0$ | | | | | | | | | | | | | | | | | | | | | — | 2 | 11 |
| $K^+\pi^-, K^0_S\eta$ | | | | | | | | | | | | | | | | | | | | | | — | 1 |
| $K^+\pi^-, K^0_S\omega$ | | | | | | | | | | | | | | | | | | | | | | | — |


[3] L. M. Zhang *et al.* [BELLE Collaboration], Phys. Rev. Lett. **99**, 131803 (2007) [arXiv:0704.1000 [hep-ex]].

[4] B. Aubert *et al.* [BABAR Collaboration], Phys. Rev. Lett. **98**, 211802 (2007) [arXiv:hep-ex/0703020].

[5] R. L. Kingsley, S. B. Treiman, F. Wilczek and A. Zee, Phys. Rev. D **11**, 1919 (1975).

[6] L. B. Okun, B. M. Pontecorvo and V. I. Zakharov, Lett. Nuovo Cim. **13**, 218 (1975).

[7] R. L. Kingsley, Phys. Lett. B **63**, 329 (1976).

[8] M. Goldhaber and J. L. Rosner, Phys. Rev. D **15**, 1254 (1977).

[9] I. I. Bigi and A. I. Sanda, Phys. Lett. B **171**, 320 (1986).

[10] I. I. Bigi, SLAC-PUB-4000. *Invited talk given at Workshop on Physics Simulation at High Energies, Madison, WI, May 5-16, 1986.*

TABLE XXV: Correlation coefficients (%), with statistical and systematic uncertainties, for the efficiency-corrected, background-subtracted yields in Tables XXII and XXIII.

| | $K^+K^-, K^+K^-$ | $K^+K^-, \pi^+\pi^-$ | $K^+K^-, K^0_S\pi^0\pi^0$ | $K^+K^-, K^0_S\pi^0$ | $K^+K^-, K^0_S\eta$ | $K^+K^-, K^0_S\omega$ | $\pi^+\pi^-, \pi^+\pi^-$ | $\pi^+\pi^-, K^0_S\pi^0\pi^0$ | $\pi^+\pi^-, K^0_S\pi^0$ | $\pi^+\pi^-, K^0_S\eta$ | $\pi^+\pi^-, K^0_S\omega$ | $K^0_S\pi^0\pi^0, K^0_S\pi^0\pi^0$ | $K^0_S\pi^0\pi^0, K^0_S\pi^0$ | $K^0_S\pi^0\pi^0, K^0_S\eta$ | $K^0_S\pi^0\pi^0, K^0_S\omega$ | $K^0_S\pi^0, K^0_S\pi^0$ | $K^0_S\pi^0, K^0_S\eta$ | $K^0_S\pi^0, K^0_S\omega$ | $K^0_S\eta, K^0_S\eta$ | $K^0_S\eta, K^0_S\omega$ | $K^0_S\omega, K^0_S\omega$ |
|---|---|---|---|---|---|---|---|---|---|---|---|---|---|---|---|---|---|---|---|---|---|
| $K^-\pi^+$ | −0 | −0 | 0 | 7 | 3 | 6 | −0 | 0 | 6 | 2 | 6 | 0 | 2 | 0 | 3 | 0 | 0 | 1 | −0 | 0 | 1 |
| $K^+\pi^-$ | −0 | −0 | 0 | 7 | 3 | 6 | −0 | 0 | 6 | 2 | 6 | 0 | 2 | 0 | 3 | 0 | 0 | 1 | −0 | 0 | 1 |
| $K^+K^-$ | 6 | 2 | 1 | 13 | 5 | 9 | −0 | 0 | 3 | 1 | 3 | 0 | 1 | 0 | 2 | 0 | 0 | 1 | −0 | 0 | 0 |
| $\pi^+\pi^-$ | −0 | 2 | 0 | 2 | 1 | 2 | 11 | 1 | 8 | 3 | 7 | 0 | 1 | 0 | 2 | 0 | 0 | 0 | −0 | 0 | 0 |
| $K^0_S\pi^0\pi^0$ | −0 | −0 | 1 | 19 | 1 | 11 | −0 | 0 | 13 | 1 | 10 | 1 | 42 | 9 | 33 | 2 | 0 | 6 | −0 | 0 | 2 |
| $K^0_S\pi^0$ | −0 | −0 | 0 | 24 | 2 | 13 | −0 | 0 | 16 | 1 | 11 | 0 | 41 | 8 | 31 | 2 | 0 | 7 | −0 | 0 | 2 |
| $K^0_S\eta$ | −0 | −0 | 0 | 3 | 15 | 2 | −0 | 0 | 2 | 11 | 1 | 0 | 3 | 9 | 3 | 0 | 1 | 1 | 2 | 1 | 0 |
| $K^0_S\omega$ | −0 | −0 | 0 | 17 | 2 | 17 | −0 | 0 | 13 | 2 | 14 | 0 | 31 | 6 | 30 | 1 | 0 | 20 | −0 | 3 | 9 |
| $K^-\pi^+, K^-\pi^+$ | −0 | −0 | 0 | 0 | 0 | 0 | −0 | 0 | 0 | 0 | 0 | 0 | 0 | 0 | 0 | 0 | 0 | 0 | −0 | 0 | 0 |
| $K^-\pi^+, K^+\pi^-$ | −0 | −0 | 0 | 5 | 2 | 4 | −0 | 0 | 4 | 2 | 4 | 0 | 1 | 0 | 2 | 0 | 0 | 1 | −0 | 0 | 0 |
| $K^-\pi^+, K^+K^-$ | −0 | −0 | 0 | 2 | 1 | 2 | −0 | 0 | 1 | 1 | 1 | 0 | 0 | 0 | 1 | 0 | 0 | 0 | −0 | 0 | 0 |
| $K^-\pi^+, \pi^+\pi^-$ | −0 | −0 | 0 | 1 | 0 | 1 | −0 | 0 | 2 | 1 | 2 | 0 | 0 | 0 | 1 | 0 | 0 | 0 | −0 | 0 | 0 |
| $K^-\pi^+, K^0_S\pi^0\pi^0$ | −0 | −0 | 0 | 9 | 1 | 6 | −0 | 0 | 7 | 0 | 5 | 0 | 19 | 4 | 15 | 1 | 0 | 3 | −0 | 0 | 1 |
| $K^-\pi^+, K^0_S\pi^0$ | −0 | −0 | 0 | 9 | 1 | 5 | −0 | 0 | 6 | 1 | 5 | 0 | 14 | 3 | 11 | 1 | 0 | 2 | −0 | 0 | 1 |
| $K^-\pi^+, K^0_S\eta$ | −0 | −0 | 0 | 1 | 3 | 1 | −0 | 0 | 1 | 3 | 1 | 0 | 1 | 2 | 1 | 0 | 0 | 0 | −0 | 0 | 0 |
| $K^-\pi^+, K^0_S\omega$ | −0 | −0 | 0 | 7 | 1 | 6 | −0 | 0 | 5 | 1 | 5 | 0 | 11 | 2 | 11 | 0 | 0 | 8 | −0 | 1 | 3 |
| $K^+\pi^-, K^+\pi^-$ | −0 | −0 | 0 | 0 | 0 | 0 | −0 | 0 | 0 | 0 | 0 | 0 | 0 | 0 | 0 | 0 | 0 | 0 | −0 | 0 | 0 |
| $K^+\pi^-, K^+K^-$ | −0 | −0 | 0 | 3 | 1 | 2 | −0 | 0 | 1 | 1 | 2 | 0 | 0 | 0 | 1 | 0 | 0 | 0 | −0 | 0 | 0 |
| $K^+\pi^-, \pi^+\pi^-$ | −0 | −0 | 0 | 1 | 1 | 1 | −0 | 0 | 2 | 1 | 2 | 0 | 0 | 0 | 1 | 0 | 0 | 0 | −0 | 0 | 0 |
| $K^+\pi^-, K^0_S\pi^0\pi^0$ | −0 | −0 | 0 | 9 | 1 | 6 | −0 | 0 | 7 | 0 | 5 | 0 | 19 | 4 | 15 | 1 | 0 | 3 | −0 | 0 | 1 |
| $K^+\pi^-, K^0_S\pi^0$ | −0 | −0 | 0 | 9 | 1 | 6 | −0 | 0 | 7 | 1 | 5 | 0 | 15 | 3 | 12 | 1 | 0 | 3 | −0 | 0 | 1 |
| $K^+\pi^-, K^0_S\eta$ | −0 | −0 | 0 | 1 | 3 | 1 | −0 | 0 | 1 | 2 | 1 | 0 | 1 | 2 | 1 | 0 | 0 | 0 | −0 | 0 | 0 |
| $K^+\pi^-, K^0_S\omega$ | −0 | −0 | 0 | 7 | 1 | 6 | −0 | 0 | 5 | 1 | 5 | 0 | 11 | 2 | 10 | 0 | 0 | 8 | −0 | 1 | 3 |


[11] I. I. Bigi, UND-HEP-89-BIG01, also SLAC-R-343, pp. 169–195. *Given at Tau Charm Factory Workshop, Stanford, CA, May 23-27, 1989.*

[12] Z. Z. Xing, Phys. Rev. D **55**, 196 (1997) [arXiv:hep-ph/9606422].

[13] M. Gronau, Y. Grossman and J. L. Rosner, Phys. Lett. B **508**, 37 (2001) [arXiv:hep-ph/0103110].

[14] S. Bianco, F. L. Fabbri, D. Benson and I. Bigi, Riv. Nuovo Cim. **26N7**, 1 (2003) [arXiv:hep-ex/0309021].

[15] D. Atwood and A. A. Petrov, Phys. Rev. D **71**, 054032 (2005) [arXiv:hep-ph/0207165].

[16] D. M. Asner and W. M. Sun, Phys. Rev. D **73**, 034024 (2006) [Erratum-ibid. **77**, 019901(E) (2008)] [arXiv:hep-ph/0507238].

[17] Q. He *et al.* [CLEO Collaboration], Phys. Rev. Lett. **95**, 121801 (2005) [Erratum-ibid. **96**, 199903 (2006)] [arXiv:hep-ex/0504003].

TABLE XXVI: Correlation coefficients (%), with statistical and systematic uncertainties, for the efficiency-corrected, background-subtracted yields in Tables XXII and XXIII.

| | $X^+e^-\bar{\nu}_e, K^-\pi^+$ | $X^+e^-\bar{\nu}_e, K^-K^+$ | $X^+e^-\bar{\nu}_e, \pi^-\pi^+$ | $X^+e^-\bar{\nu}_e, K^0_S\pi^0\pi^0$ | $X^+e^-\bar{\nu}_e, K^0_S\pi^0$ | $X^+e^-\bar{\nu}_e, K^0_S\eta$ | $X^+e^-\bar{\nu}_e, K^0_S\omega$ | $X^-e^+\nu_e, K^+\pi^-$ | $X^-e^+\nu_e, K^-K^+$ | $X^-e^+\nu_e, \pi^-\pi^+$ | $X^-e^+\nu_e, K^0_S\pi^0\pi^0$ | $X^-e^+\nu_e, K^0_S\pi^0$ | $X^-e^+\nu_e, K^0_S\eta$ | $X^-e^+\nu_e, K^0_S\omega$ | $K^0_L\pi^0, K^-\pi^+$ | $K^0_L\pi^0, K^+\pi^-$ | $K^0_L\pi^0, K^+K^-$ | $K^0_L\pi^0, \pi^+\pi^-$ | $K^0_L\pi^0, K^0_S\pi^0\pi^0$ | $K^0_L\pi^0, K^0_S\pi^0$ | $K^0_L\pi^0, K^0_S\eta$ | $K^0_L\pi^0, K^0_S\omega$ |
|---|---|---|---|---|---|---|---|---|---|---|---|---|---|---|---|---|---|---|---|---|---|---|
| $K^-\pi^+$ | 43 | 7 | 6 | 1 | 4 | 2 | 6 | 34 | 7 | 8 | 2 | 5 | 2 | 6 | 17 | 15 | −0 | −0 | −0 | 2 | 1 | 5 |
| $K^+\pi^-$ | 36 | 7 | 6 | 1 | 4 | 2 | 6 | 43 | 7 | 8 | 2 | 5 | 2 | 6 | 15 | 18 | −0 | −0 | −0 | 2 | 1 | 5 |
| $K^+K^-$ | 22 | 28 | 3 | 1 | 3 | 1 | 3 | 22 | 27 | 4 | 1 | 3 | 1 | 3 | 9 | 10 | 0 | −0 | −0 | 2 | 1 | 3 |
| $\pi^+\pi^-$ | 14 | 2 | 18 | 1 | 2 | 1 | 3 | 13 | 2 | 17 | 1 | 2 | 1 | 3 | 5 | 6 | −0 | 2 | −0 | 1 | 0 | 3 |
| $K^0_S\pi^0\pi^0$ | 2 | 0 | 0 | 28 | 26 | 1 | 16 | 2 | 0 | 0 | 34 | 30 | 1 | 16 | 35 | 36 | −1 | −0 | 0 | 49 | 13 | 36 |
| $K^0_S\pi^0$ | 3 | 1 | 1 | 16 | 36 | 3 | 18 | 3 | 1 | 1 | 24 | 40 | 2 | 18 | 35 | 36 | −2 | −1 | −1 | 55 | 14 | 38 |
| $K^0_S\eta$ | 2 | 0 | 0 | 1 | 3 | 29 | 2 | 2 | 0 | 0 | 2 | 4 | 27 | 2 | 0 | 1 | −1 | −0 | −0 | 3 | 23 | 2 |
| $K^0_S\omega$ | 8 | 2 | 2 | 12 | 23 | 3 | 31 | 8 | 2 | 2 | 19 | 27 | 2 | 32 | 29 | 30 | −1 | −0 | −1 | 40 | 11 | 39 |
| $K^-\pi^+, K^-\pi^+$ | 0 | 0 | 0 | 0 | 0 | 0 | 0 | 0 | 0 | 0 | 0 | 0 | 0 | 0 | 0 | 0 | −0 | −0 | −0 | 0 | 0 | 0 |
| $K^-\pi^+, K^+\pi^-$ | 24 | 5 | 4 | 1 | 3 | 1 | 4 | 23 | 5 | 5 | 1 | 3 | 1 | 4 | 10 | 10 | −0 | −0 | −0 | 1 | 1 | 4 |
| $K^-\pi^+, K^+K^-$ | 8 | 2 | 1 | 0 | 1 | 0 | 1 | 8 | 2 | 2 | 0 | 1 | 0 | 1 | 3 | 4 | −0 | −0 | −0 | 0 | 0 | 1 |
| $K^-\pi^+, \pi^+\pi^-$ | 7 | 1 | 2 | 0 | 1 | 0 | 1 | 7 | 1 | 3 | 0 | 1 | 0 | 1 | 3 | 3 | −0 | −0 | −0 | 0 | 0 | 1 |
| $K^-\pi^+, K^0_S\pi^0\pi^0$ | 4 | 1 | 1 | 8 | 12 | 1 | 8 | 4 | 1 | 1 | 12 | 14 | 1 | 8 | 17 | 18 | −0 | −0 | −0 | 23 | 6 | 17 |
| $K^-\pi^+, K^0_S\pi^0$ | 6 | 1 | 1 | 6 | 11 | 1 | 7 | 5 | 1 | 1 | 9 | 12 | 1 | 7 | 8 | 14 | −0 | −0 | −0 | 18 | 5 | 14 |
| $K^-\pi^+, K^0_S\eta$ | 2 | 0 | 0 | 0 | 1 | 5 | 1 | 2 | 0 | 1 | 0 | 1 | 5 | 1 | 1 | 1 | −0 | −0 | −0 | 1 | 5 | 1 |
| $K^-\pi^+, K^0_S\omega$ | 6 | 1 | 1 | 4 | 8 | 1 | 9 | 6 | 1 | 2 | 7 | 10 | 1 | 9 | 12 | 12 | −0 | −0 | −0 | 14 | 4 | 13 |
| $K^+\pi^-, K^+\pi^-$ | 0 | 0 | 0 | 0 | 0 | 0 | 0 | 0 | 0 | 0 | 0 | 0 | 0 | 0 | 0 | 0 | −0 | −0 | −0 | 0 | 0 | 0 |
| $K^+\pi^-, K^+K^-$ | 10 | 3 | 2 | 0 | 1 | 1 | 1 | 9 | 3 | 2 | 0 | 1 | 0 | 1 | 4 | 4 | −0 | −0 | −0 | 1 | 0 | 1 |
| $K^+\pi^-, \pi^+\pi^-$ | 7 | 1 | 2 | 0 | 1 | 0 | 1 | 7 | 1 | 3 | 0 | 1 | 0 | 1 | 3 | 3 | −0 | −0 | −0 | 0 | 0 | 1 |
| $K^+\pi^-, K^0_S\pi^0\pi^0$ | 4 | 1 | 1 | 8 | 12 | 1 | 8 | 4 | 1 | 1 | 12 | 14 | 1 | 8 | 17 | 18 | −0 | −0 | −0 | 22 | 6 | 17 |
| $K^+\pi^-, K^0_S\pi^0$ | 6 | 1 | 1 | 6 | 12 | 1 | 8 | 6 | 1 | 1 | 9 | 14 | 1 | 8 | 15 | 10 | −0 | −0 | −0 | 20 | 5 | 15 |
| $K^+\pi^-, K^0_S\eta$ | 2 | 0 | 0 | 0 | 1 | 5 | 1 | 2 | 0 | 1 | 0 | 1 | 5 | 1 | 1 | 1 | −0 | −0 | −0 | 1 | 5 | 1 |
| $K^+\pi^-, K^0_S\omega$ | 6 | 1 | 1 | 4 | 8 | 1 | 9 | 6 | 1 | 1 | 7 | 9 | 1 | 9 | 11 | 12 | −0 | −0 | −0 | 14 | 4 | 13 |


[18] W. M. Sun, Nucl. Instrum. Meth. A **556**, 325 (2006) [arXiv:physics/0503050].

[19] Y. Kubota *et al.*, Nucl. Instrum. Meth. A **320**, 66 (1992).

[20] T. S. Hill, Nucl. Instrum. Meth. A **418**, 32 (1998).

[21] D. Peterson *et al.*, Nucl. Instrum. Meth. A **478**, 142 (2002).

[22] M. Artuso *et al.*, Nucl. Instrum. Meth. A **502**, 91 (2003);

[23] R.A. Briere *et al.* [CLEO-c/CESR-c Taskforces & CLEO-c Collaboration], Cornell LEPP preprint CLNS 01/1742 (2001).

[24] S. Dobbs *et al.* [CLEO Collaboration], Phys. Rev. D **76**, 112001 (2007) [arXiv:0709.3783 [hep-ex]].

[25] W.-M. Yao *et al.*, Journal of Physics G **33**, 1 (2006).

[26] H. Albrecht *et al.* (ARGUS Collaboration), Phys. Lett. B **241**, 278 (1990).

[27] T. E. Coan *et al.* [CLEO Collaboration], Phys. Rev. Lett. **95**, 181802 (2005) [arXiv:hep-

TABLE XXVII: Correlation coefficients (%), with statistical and systematic uncertainties, for the efficiency-corrected, background-subtracted yields in Tables XXII and XXIII. Coefficients of 100% are represented by a dash (—).

| | $K^+K^-, K^+K^-$ | $K^+K^-, \pi^+\pi^-$ | $K^+K^-, K^0_S\pi^0\pi^0$ | $K^+K^-, K^0_S\pi^0$ | $K^+K^-, K^0_S\eta$ | $K^+K^-, K^0_S\omega$ | $\pi^+\pi^-, \pi^+\pi^-$ | $\pi^+\pi^-, K^0_S\pi^0\pi^0$ | $\pi^+\pi^-, K^0_S\pi^0$ | $\pi^+\pi^-, K^0_S\eta$ | $\pi^+\pi^-, K^0_S\omega$ | $K^0_S\pi^0\pi^0, K^0_S\pi^0\pi^0$ | $K^0_S\pi^0\pi^0, K^0_S\pi^0$ | $K^0_S\pi^0\pi^0, K^0_S\eta$ | $K^0_S\pi^0\pi^0, K^0_S\omega$ | $K^0_S\pi^0, K^0_S\pi^0$ | $K^0_S\pi^0, K^0_S\eta$ | $K^0_S\pi^0, K^0_S\omega$ | $K^0_S\eta, K^0_S\eta$ | $K^0_S\eta, K^0_S\omega$ | $K^0_S\omega, K^0_S\omega$ |
|---|---|---|---|---|---|---|---|---|---|---|---|---|---|---|---|---|---|---|---|---|---|
| $K^+K^-, K^+K^-$ | — | 0 | −0 | −0 | −0 | −0 | 0 | −0 | −0 | −0 | −0 | −0 | −0 | −0 | −0 | −0 | −0 | −0 | 0 | −0 | −0 |
| $K^+K^-, \pi^+\pi^-$ | | — | −0 | −0 | −0 | −0 | 0 | 0 | −0 | −0 | −0 | −0 | −0 | −0 | −0 | −0 | −0 | −0 | 0 | −0 | −0 |
| $K^+K^-, K^0_S\pi^0\pi^0$ | | | — | 0 | 0 | 0 | −0 | 0 | 0 | 0 | 0 | 0 | 0 | 0 | 0 | 0 | 0 | 0 | −0 | 0 | 0 |
| $K^+K^-, K^0_S\pi^0$ | | | | — | 1 | 4 | −0 | 0 | 4 | 0 | 3 | 0 | 10 | 2 | 8 | 0 | 0 | 2 | −0 | 0 | 1 |
| $K^+K^-, K^0_S\eta$ | | | | | — | 1 | −0 | 0 | 0 | 1 | 0 | 0 | 1 | 1 | 0 | 0 | 0 | 0 | −0 | 0 | 0 |
| $K^+K^-, K^0_S\omega$ | | | | | | — | −0 | 0 | 2 | 0 | 2 | 0 | 6 | 1 | 5 | 0 | 0 | 2 | −0 | 0 | 1 |
| $\pi^+\pi^-, \pi^+\pi^-$ | | | | | | | — | 0 | −0 | −0 | −0 | −0 | −0 | −0 | −0 | −0 | −0 | −0 | 0 | −0 | −0 |
| $\pi^+\pi^-, K^0_S\pi^0\pi^0$ | | | | | | | | — | 0 | 0 | 0 | 0 | 0 | 0 | 0 | 0 | 0 | 0 | −0 | 0 | 0 |
| $\pi^+\pi^-, K^0_S\pi^0$ | | | | | | | | | — | 1 | 3 | 0 | 7 | 1 | 5 | 0 | 0 | 1 | −0 | 0 | 0 |
| $\pi^+\pi^-, K^0_S\eta$ | | | | | | | | | | — | 0 | 0 | 0 | 1 | 0 | 0 | 0 | 0 | −0 | 0 | 0 |
| $\pi^+\pi^-, K^0_S\omega$ | | | | | | | | | | | — | 0 | 5 | 1 | 4 | 0 | 0 | 2 | −0 | 0 | 1 |
| $K^0_S\pi^0\pi^0, K^0_S\pi^0\pi^0$ | | | | | | | | | | | | — | 0 | 0 | 0 | 0 | 0 | 0 | −0 | 0 | 0 |
| $K^0_S\pi^0\pi^0, K^0_S\pi^0$ | | | | | | | | | | | | | — | 4 | 15 | 1 | 0 | 3 | −0 | 0 | 1 |
| $K^0_S\pi^0\pi^0, K^0_S\eta$ | | | | | | | | | | | | | | — | 3 | 0 | 0 | 1 | −0 | 0 | 0 |
| $K^0_S\pi^0\pi^0, K^0_S\omega$ | | | | | | | | | | | | | | | — | 1 | 0 | 4 | −0 | 0 | 2 |
| $K^0_S\pi^0, K^0_S\pi^0$ | | | | | | | | | | | | | | | | — | 0 | 0 | −0 | 0 | 0 |
| $K^0_S\pi^0, K^0_S\eta$ | | | | | | | | | | | | | | | | | — | 0 | −0 | 0 | 0 |
| $K^0_S\pi^0, K^0_S\omega$ | | | | | | | | | | | | | | | | | | — | −0 | 1 | 4 |
| $K^0_S\eta, K^0_S\eta$ | | | | | | | | | | | | | | | | | | | — | −0 | −0 |
| $K^0_S\eta, K^0_S\omega$ | | | | | | | | | | | | | | | | | | | | — | 1 |
| $K^0_S\omega, K^0_S\omega$ | | | | | | | | | | | | | | | | | | | | | — |


ex/0506052].

[28] Q. He *et al.* [CLEO Collaboration], arXiv:0711.1463 [hep-ex].

[29] S. Eidelman *et al.*, Phys. Lett. B **592**, 1 (2004).

[30] E. M. Aitala *et al.* [E791 Collaboration], Phys. Lett. B **421**, 405 (1998) [arXiv:hep-ex/9711003].

[31] S. E. Csorna *et al.* [CLEO Collaboration], Phys. Rev. D **65**, 092001 (2002) [arXiv:hep-ex/0111024].

[32] J. M. Link *et al.* [FOCUS Collaboration], Phys. Lett. B **555**, 167 (2003) [arXiv:hep-ex/0212058].

[33] D. Acosta *et al.* [CDF Collaboration], Phys. Rev. Lett. **94**, 122001 (2005) [arXiv:hep-ex/0504006].

[34] P. Rubin *et al.* [CLEO Collaboration], Phys. Rev. Lett. **96**, 081802 (2006) [arXiv:hep-ex/0512063].

[35] E. M. Aitala *et al.* [E791 Collaboration], Phys. Rev. D **57**, 13 (1998) [arXiv:hep-ex/9608018].

TABLE XXVIII: Correlation coefficients (%), with statistical and systematic uncertainties, for the efficiency-corrected, background-subtracted yields in Tables XXII and XXIII.

| | $X^+e^-\bar{\nu}_e, K^-\pi^+$ | $X^+e^-\bar{\nu}_e, K^-K^+$ | $X^+e^-\bar{\nu}_e, \pi^-\pi^+$ | $X^+e^-\bar{\nu}_e, K^0_S\pi^0\pi^0$ | $X^+e^-\bar{\nu}_e, K^0_S\pi^0$ | $X^+e^-\bar{\nu}_e, K^0_S\eta$ | $X^+e^-\bar{\nu}_e, K^0_S\omega$ | $X^-e^+\nu_e, K^+\pi^-$ | $X^-e^+\nu_e, K^-K^+$ | $X^-e^+\nu_e, \pi^-\pi^+$ | $X^-e^+\nu_e, K^0_S\pi^0\pi^0$ | $X^-e^+\nu_e, K^0_S\pi^0$ | $X^-e^+\nu_e, K^0_S\eta$ | $X^-e^+\nu_e, K^0_S\omega$ | $K^0_L\pi^0, K^-\pi^+$ | $K^0_L\pi^0, K^+\pi^-$ | $K^0_L\pi^0, K^+K^-$ | $K^0_L\pi^0, \pi^+\pi^-$ | $K^0_L\pi^0, K^0_S\pi^0\pi^0$ | $K^0_L\pi^0, K^0_S\pi^0$ | $K^0_L\pi^0, K^0_S\eta$ | $K^0_L\pi^0, K^0_S\omega$ |
|---|---|---|---|---|---|---|---|---|---|---|---|---|---|---|---|---|---|---|---|---|---|---|
| $K^+K^-, K^+K^-$ | −0 | −0 | −0 | −0 | −0 | −0 | −0 | −0 | −0 | −0 | −0 | −0 | −0 | −0 | −0 | −0 | 0 | 0 | 0 | −0 | −0 | −0 |
| $K^+K^-, \pi^+\pi^-$ | −0 | −0 | −0 | −0 | −0 | −0 | −0 | −0 | −0 | −0 | −0 | −0 | −0 | −0 | −0 | −0 | 0 | 0 | 0 | −0 | −0 | −0 |
| $K^+K^-, K^0_S\pi^0\pi^0$ | 0 | 0 | 0 | 0 | 0 | 0 | 0 | 0 | 0 | 0 | 0 | 0 | 0 | 0 | 0 | 0 | −0 | −0 | −0 | 0 | 0 | 0 |
| $K^+K^-, K^0_S\pi^0$ | 3 | 1 | 0 | 4 | 7 | 1 | 5 | 3 | 1 | 1 | 6 | 8 | 1 | 5 | 9 | 10 | −27 | −0 | −0 | 13 | 3 | 9 |
| $K^+K^-, K^0_S\eta$ | 1 | 0 | 0 | 0 | 1 | 3 | 0 | 1 | 0 | 0 | 0 | 1 | 3 | 0 | 0 | 1 | −0 | −0 | −0 | 1 | 3 | 1 |
| $K^+K^-, K^0_S\omega$ | 3 | 1 | 1 | 2 | 4 | 1 | 4 | 3 | 1 | 1 | 3 | 5 | 0 | 4 | 6 | 6 | −0 | −0 | −0 | 7 | 2 | 6 |
| $\pi^+\pi^-, \pi^+\pi^-$ | −0 | −0 | −0 | −0 | −0 | −0 | −0 | −0 | −0 | −0 | −0 | −0 | −0 | −0 | −0 | −0 | 0 | 0 | 0 | −0 | −0 | −0 |
| $\pi^+\pi^-, K^0_S\pi^0\pi^0$ | 0 | 0 | −0 | 0 | 0 | 0 | 0 | 0 | 0 | −0 | 0 | 0 | 0 | 0 | 0 | 0 | −0 | −0 | −0 | 0 | 0 | 0 |
| $\pi^+\pi^-, K^0_S\pi^0$ | 3 | 0 | 1 | 3 | 5 | 1 | 3 | 3 | 0 | 1 | 4 | 6 | 0 | 3 | 7 | 7 | −0 | −18 | −0 | 9 | 2 | 7 |
| $\pi^+\pi^-, K^0_S\eta$ | 1 | 0 | 0 | 0 | 0 | 2 | 0 | 1 | 0 | 1 | 0 | 1 | 2 | 0 | 0 | 0 | −0 | −0 | −0 | 0 | 2 | 0 |
| $\pi^+\pi^-, K^0_S\omega$ | 3 | 0 | 1 | 2 | 4 | 0 | 3 | 3 | 0 | 1 | 3 | 4 | 0 | 3 | 5 | 5 | −0 | −0 | −0 | 6 | 2 | 6 |
| $K^0_S\pi^0\pi^0, K^0_S\pi^0\pi^0$ | 0 | 0 | 0 | 0 | 0 | 0 | 0 | 0 | 0 | 0 | 0 | 0 | 0 | 0 | 0 | 0 | −0 | −0 | −0 | 0 | 0 | 0 |
| $K^0_S\pi^0\pi^0, K^0_S\pi^0$ | 1 | 0 | 0 | 8 | 13 | 1 | 8 | 1 | 0 | 0 | 12 | 15 | 1 | 8 | 17 | 17 | −0 | −0 | −21 | 24 | 6 | 17 |
| $K^0_S\pi^0\pi^0, K^0_S\eta$ | 0 | 0 | 0 | 2 | 3 | 2 | 2 | 0 | 0 | 0 | 2 | 3 | 1 | 2 | 3 | 3 | −0 | −0 | −0 | 5 | 3 | 3 |
| $K^0_S\pi^0\pi^0, K^0_S\omega$ | 2 | 0 | 0 | 6 | 10 | 1 | 7 | 2 | 0 | 0 | 9 | 12 | 1 | 8 | 13 | 14 | −0 | −0 | −0 | 19 | 5 | 15 |
| $K^0_S\pi^0, K^0_S\pi^0$ | 0 | 0 | 0 | 0 | 1 | 0 | 0 | 0 | 0 | 0 | 0 | 1 | 0 | 0 | 1 | 1 | −0 | −0 | −0 | 1 | 0 | 1 |
| $K^0_S\pi^0, K^0_S\eta$ | 0 | 0 | 0 | 0 | 0 | 0 | 0 | 0 | 0 | 0 | 0 | 0 | 0 | 0 | 0 | 0 | −0 | −0 | −0 | 0 | 0 | 0 |
| $K^0_S\pi^0, K^0_S\omega$ | 0 | 0 | 0 | 1 | 2 | 0 | 5 | 0 | 0 | 0 | 2 | 2 | 0 | 5 | 3 | 3 | −0 | −0 | −0 | 4 | 1 | 5 |
| $K^0_S\eta, K^0_S\eta$ | −0 | −0 | −0 | −0 | −0 | −0 | −0 | −0 | −0 | −0 | −0 | −0 | −0 | −0 | −0 | −0 | 0 | 0 | 0 | −0 | −0 | −0 |
| $K^0_S\eta, K^0_S\omega$ | 0 | 0 | 0 | 0 | 0 | 0 | 1 | 0 | 0 | 0 | 0 | 0 | 0 | 1 | 0 | 0 | −0 | −0 | −0 | 0 | 0 | 1 |
| $K^0_S\omega, K^0_S\omega$ | 0 | 0 | 0 | 0 | 1 | 0 | 2 | 0 | 0 | 0 | 1 | 1 | 0 | 2 | 1 | 1 | −0 | −0 | −0 | 1 | 0 | 2 |


[36] J. M. Link *et al.* [FOCUS Collaboration], Phys. Lett. B **618**, 23 (2005) [arXiv:hep-ex/0412034].

[37] A. Abulencia *et al.* [CDF Collaboration], Phys. Rev. D **74**, 031109 (2006) [arXiv:hep-ex/0605027].

[38] E. M. Aitala *et al.* [E791 Collaboration], Phys. Rev. Lett. **77**, 2384 (1996) [arXiv:hep-ex/9606016].

[39] C. Cawlfield *et al.* [CLEO Collaboration], Phys. Rev. D **71**, 077101 (2005) [arXiv:hep-ex/0502012].

[40] K. Abe *et al.* [Belle Collaboration], Phys. Rev. D **72**, 071101 (2005) [arXiv:hep-ex/0507020].

[41] B. Aubert *et al.* [BABAR Collaboration], Phys. Rev. D **76**, 014018 (2007) [arXiv:0705.0704 [hep-ex]].

[42] E. M. Aitala *et al.* [E791 Collaboration], Phys. Rev. Lett. **83**, 32 (1999) [arXiv:hep-ex/9903012].

[43] J. M. Link *et al.* [FOCUS Collaboration], Phys. Lett. B **485**, 62 (2000) [arXiv:hep-ex/0004034].

[44] B. Aubert *et al.* [BABAR Collaboration], Phys. Rev. Lett. **91**, 121801 (2003) [arXiv:hep-

TABLE XXIX: Correlation coefficients (%), with statistical and systematic uncertainties, for the efficiency-corrected, background-subtracted yields in Tables XXII and XXIII. Coefficients of 100% are represented by a dash (—).

| | $X^+e^-\bar{\nu}_e, K^-\pi^+$ | $X^+e^-\bar{\nu}_e, K^-K^+$ | $X^+e^-\bar{\nu}_e, \pi^-\pi^+$ | $X^+e^-\bar{\nu}_e, K^0_S\pi^0\pi^0$ | $X^+e^-\bar{\nu}_e, K^0_S\pi^0$ | $X^+e^-\bar{\nu}_e, K^0_S\eta$ | $X^+e^-\bar{\nu}_e, K^0_S\omega$ | $X^-e^+\nu_e, K^+\pi^-$ | $X^-e^+\nu_e, K^-K^+$ | $X^-e^+\nu_e, \pi^-\pi^+$ | $X^-e^+\nu_e, K^0_S\pi^0\pi^0$ | $X^-e^+\nu_e, K^0_S\pi^0$ | $X^-e^+\nu_e, K^0_S\eta$ | $X^-e^+\nu_e, K^0_S\omega$ | $K^0_L\pi^0, K^-\pi^+$ | $K^0_L\pi^0, K^+\pi^-$ | $K^0_L\pi^0, K^+K^-$ | $K^0_L\pi^0, \pi^+\pi^-$ | $K^0_L\pi^0, K^0_S\pi^0\pi^0$ | $K^0_L\pi^0, K^0_S\pi^0$ | $K^0_L\pi^0, K^0_S\eta$ | $K^0_L\pi^0, K^0_S\omega$ |
|---|---|---|---|---|---|---|---|---|---|---|---|---|---|---|---|---|---|---|---|---|---|---|
| $X^+e^-\bar{\nu}_e, K^-\pi^+$ | — | 8 | 6 | 3 | 9 | 4 | 7 | 36 | 8 | 8 | 4 | 10 | 4 | 7 | 7 | 7 | −0 | −0 | −0 | 1 | 1 | 3 |
| $X^+e^-\bar{\nu}_e, K^-K^+$ | | — | 1 | 1 | 2 | 1 | 1 | 8 | 2 | 2 | 1 | 2 | 1 | 1 | 1 | 1 | −0 | −0 | −0 | 0 | 0 | 0 |
| $X^+e^-\bar{\nu}_e, \pi^-\pi^+$ | | | — | 0 | 2 | 1 | 1 | 6 | 1 | 2 | 1 | 2 | 1 | 1 | 1 | 1 | −0 | −0 | −0 | 0 | 0 | 1 |
| $X^+e^-\bar{\nu}_e, K^0_S\pi^0\pi^0$ | | | | — | 6 | 1 | 4 | 3 | 1 | 1 | 5 | 7 | 1 | 4 | 7 | 7 | −0 | −0 | −0 | 10 | 2 | 7 |
| $X^+e^-\bar{\nu}_e, K^0_S\pi^0$ | | | | | — | 2 | 7 | 9 | 2 | 2 | 9 | 14 | 2 | 7 | 12 | 12 | −0 | −0 | −0 | 17 | 5 | 12 |
| $X^+e^-\bar{\nu}_e, K^0_S\eta$ | | | | | | — | 1 | 4 | 1 | 1 | 1 | 2 | 5 | 1 | 0 | 0 | −0 | −0 | −0 | 1 | 6 | 1 |
| $X^+e^-\bar{\nu}_e, K^0_S\omega$ | | | | | | | — | 7 | 1 | 2 | 6 | 8 | 1 | 7 | 8 | 8 | −0 | −0 | −0 | 10 | 3 | 9 |
| $X^-e^+\nu_e, K^+\pi^-$ | | | | | | | | — | 8 | 8 | 4 | 10 | 4 | 7 | 6 | 6 | −0 | −0 | −0 | 1 | 0 | 2 |
| $X^-e^+\nu_e, K^-K^+$ | | | | | | | | | — | 2 | 1 | 2 | 1 | 1 | 1 | 1 | −0 | −0 | −0 | 0 | 0 | 0 |
| $X^-e^+\nu_e, \pi^-\pi^+$ | | | | | | | | | | — | 1 | 2 | 1 | 2 | 1 | 1 | −0 | −0 | −0 | 0 | 0 | 1 |
| $X^-e^+\nu_e, K^0_S\pi^0\pi^0$ | | | | | | | | | | | — | 10 | 1 | 6 | 11 | 11 | −0 | −0 | −0 | 15 | 4 | 11 |
| $X^-e^+\nu_e, K^0_S\pi^0$ | | | | | | | | | | | | — | 2 | 9 | 13 | 14 | −0 | −0 | −0 | 20 | 5 | 14 |
| $X^-e^+\nu_e, K^0_S\eta$ | | | | | | | | | | | | | — | 1 | 0 | 0 | −0 | −0 | −0 | 1 | 5 | 1 |
| $X^-e^+\nu_e, K^0_S\omega$ | | | | | | | | | | | | | | — | 8 | 8 | −0 | −0 | −0 | 10 | 3 | 10 |
| $K^0_L\pi^0, K^-\pi^+$ | | | | | | | | | | | | | | | — | 25 | −0 | −0 | 0 | 26 | 7 | 19 |
| $K^0_L\pi^0, K^+\pi^-$ | | | | | | | | | | | | | | | | — | −0 | −0 | 0 | 26 | 7 | 20 |
| $K^0_L\pi^0, K^+K^-$ | | | | | | | | | | | | | | | | | — | 0 | 0 | −0 | −0 | −0 |
| $K^0_L\pi^0, \pi^+\pi^-$ | | | | | | | | | | | | | | | | | | — | 0 | −0 | −0 | −0 |
| $K^0_L\pi^0, K^0_S\pi^0\pi^0$ | | | | | | | | | | | | | | | | | | | — | −0 | −0 | −0 |
| $K^0_L\pi^0, K^0_S\pi^0$ | | | | | | | | | | | | | | | | | | | | — | 9 | 24 |
| $K^0_L\pi^0, K^0_S\eta$ | | | | | | | | | | | | | | | | | | | | | — | 7 |
| $K^0_L\pi^0, K^0_S\omega$ | | | | | | | | | | | | | | | | | | | | | | — |


ex/0306003].

[45] K. Abe *et al.* [Belle Collaboration], Phys. Rev. Lett. **88**, 162001 (2002) [arXiv:hep-ex/0111026].

[46] M. Staric *et al.* [Belle Collaboration], Phys. Rev. Lett. **98**, 211803 (2007) [arXiv:hep-ex/0703036].

[47] D. M. Asner *et al.* [CLEO Collaboration], Phys. Rev. D **72**, 012001 (2005) [arXiv:hep-ex/0503045].

[48] R. Godang *et al.* [CLEO Collaboration], Phys. Rev. Lett. **84**, 5038 (2000) [arXiv:hep-ex/0001060].

[49] J. Alexander *et al.* [CLEO Collaboration], arXiv:0801.0680 [hep-ex].

[50] E. Barberio and Z. Was, Comput. Phys. Commun. **79**, 291 (1994).

[51] A. Petrov, private communication.

TABLE XXX: Results from the fit with external inputs from Table X, but not Tables XI or XII. Uncertainties are statistical and systematic, respectively. Charge-averaged $D^0$ branching fractions are denoted by final state.

| Parameter | Fitted Value |
|---|---|
| $\mathcal{N}$ $(10^6)$ | $1.062 \pm 0.024 \pm 0.011$ |
| $y$ $(10^{-3})$ | $-52 \pm 60 \pm 17$ |
| $r^2$ $(10^{-3})$ | $-24 \pm 16 \pm 12$ |
| $r\cos\delta$ | $0.089 \pm 0.036 \pm 0.009$ |
| $R_{\rm M}$ $(10^{-3})$ | $2.0 \pm 1.2 \pm 1.2$ |
| $rx\sin\delta$ $(10^{-3})$ | 0 (fixed) |
| $\mathcal{B}(K^-\pi^+)$ (%) | $3.81 \pm 0.05 \pm 0.06$ |
| $\mathcal{B}(K^-K^+)$ $(10^{-3})$ | $3.86 \pm 0.06 \pm 0.06$ |
| $\mathcal{B}(\pi^-\pi^+)$ $(10^{-3})$ | $1.37 \pm 0.02 \pm 0.03$ |
| $\mathcal{B}(K^0_S\pi^0\pi^0)$ $(10^{-3})$ | $8.27 \pm 0.45 \pm 0.41$ |
| $\mathcal{B}(K^0_S\pi^0)$ (%) | $1.13 \pm 0.03 \pm 0.03$ |
| $\mathcal{B}(K^0_S\eta)$ $(10^{-3})$ | $4.36 \pm 0.15 \pm 0.27$ |
| $\mathcal{B}(K^0_S\omega)$ (%) | $1.10 \pm 0.04 \pm 0.05$ |
| $\mathcal{B}(X^-e^+\nu_e)$ (%) | $6.35 \pm 0.19 \pm 0.18$ |
| $\mathcal{B}(K^0_L\pi^0)$ (%) | $1.02 \pm 0.03 \pm 0.02$ |
| $\chi^2_{\rm fit}$/ndof | 26.1/44 |

TABLE XXXI: Correlation coefficients (%) for the fit in Table XXX using both statistical and systematic uncertainties.

| | $y$ | $r^2$ | $r\cos\delta$ | $R_{\rm M}$ | $K^-\pi^+$ | $K^-K^+$ | $\pi^-\pi^+$ | $K^0_S\pi^0\pi^0$ | $K^0_S\pi^0$ | $K^0_S\eta$ | $K^0_S\omega$ | $X^-e^+\nu_e$ | $K^0_L\pi^0$ |
|---|---|---|---|---|---|---|---|---|---|---|---|---|---|
| $\mathcal{N}$ | −13 | −37 | −3 | 5 | −44 | −60 | −46 | −17 | −46 | −27 | −28 | −17 | 37 |
| $y$ | | −32 | −83 | −6 | −23 | 12 | 7 | −0 | −4 | 2 | −3 | 30 | 7 |
| $r^2$ | | | 39 | 1 | −16 | 7 | −6 | 8 | 23 | 11 | 20 | 29 | −20 |
| $r\cos\delta$ | | | | 6 | 23 | −3 | −1 | 12 | 21 | 4 | 13 | −21 | −22 |
| $R_{\rm M}$ | | | | | −9 | −3 | −3 | −0 | −1 | −1 | −1 | −2 | 1 |
| $K^-\pi^+$ | | | | | | 72 | 74 | 10 | 27 | 14 | 21 | −16 | −22 |
| $K^-K^+$ | | | | | | | 73 | 12 | 31 | 18 | 24 | 9 | −25 |
| $\pi^-\pi^+$ | | | | | | | | 9 | 25 | 14 | 20 | −0 | −19 |
| $K^0_S\pi^0\pi^0$ | | | | | | | | | 64 | 15 | 46 | 3 | −37 |
| $K^0_S\pi^0$ | | | | | | | | | | 31 | 59 | 8 | −66 |
| $K^0_S\eta$ | | | | | | | | | | | 20 | 5 | −22 |
| $K^0_S\omega$ | | | | | | | | | | | | 9 | −38 |
| $X^-e^+\nu_e$ | | | | | | | | | | | | | −5 |